The Shelf Circulation of the Bellingshausen Sea

L. M. Schulze Chretien[1], A. F. Thompson[2], M. M. Flexas[2], K. Speer[3], N. Swaim[1], R. Oelerich[4], X. Ruan[5]. R. Schubert[3], C. LoBuglio[1]

[1]Marine Science Research Institute, Department of Biology and Marine Science, Jacksonville University, Jacksonville, Florida
[2]Environmental Science and Engineering, California Institute of Technology, Pasadena, California
[3]Geophysical Fluid Dynamics Institute, Department of Earth, Ocean, and Atmospheric Science, Florida State University, Tallahassee, Florida
[5]Department of Earth, Atmospheric, and Planetary Sciences, Massachusetts Institute of Technology, Cambridge, Massachusetts
[4]Centre for Ocean and Atmospheric Sciences, School of Environmental Sciences, University of East Anglia, Norwich, United Kingdom.

Key Points:

- Warm Circumpolar Deep Water is transported onto the Bellingshausen Sea shelf along the eastern side of the Belgica and Latady Troughs.
- Meltwater leaves the region towards the west and is exported from the shelf along the western sides of the troughs, with parts of the Latady meltwater recirculating into the Belgica Trough.
- Observations indicate heat transport onto the shelf that is comparable with other regions, as well as a possible pathway connecting the West Antarctic Peninsula with the Amundsen Sea via the Bellingshausen Sea.

Corresponding author: Lena M. Schulze Chretien, `lschulz2@ju.edu`, `Marine Science Research Institute, Department of Biology and Marine Science, Jacksonville University`

Abstract

Over recent decades, the West Antarctic Ice Sheet has experienced rapid thinning of floating ice shelves as well as retreating grounding lines across its marine-terminating glaciers. The transport of warm Circumpolar Deep Water (CDW) onto the continental shelf, extensively documented in the West Antarctic Peninsula (WAP) and the Amundsen Sea, has been identified as the key process for inducing these changes. The Bellingshausen Sea sits between the WAP and the Amundsen Sea and has exhibited similar rates of ice shelf thinning, yet remains remarkably under-studied compared to regions to the east and west. We present observations collected from a hydrographic survey of the Bellingshausen Sea continental shelf completed in early 2019. Using a combination of CTD, lowered ADCP observations, as well as measurements from ocean gliders, we show that submarine troughs provide topographically-steered pathways for CDW from the shelf break towards deep embayments and ultimately under floating ice shelves. Warm, modified CDW enters the shelf at the deepest part of the Belgica Trough and flows onshore along the eastern side of the trough. Modification of these poleward-flowing waters can be detected both at the western edge of the Latady and Belgica Troughs. Modified waters from the Latady Trough recirculate in the Belgica Trough, whereas modified waters leave the Bellingshausen Sea and flow west upon leaving the Belgica Trough. Our results show that this region is a critical part of the larger West Antarctic circulation system, linking the WAP and the Amundsen Sea.

1 Introduction

Oceanic processes in the Southern Ocean and along the Antarctic margins influence climate change on a global scale. The Southern Ocean has persistently warmed over the last century (Gille, 2008), which has been accompanied by an increase in heat content of the West Antarctic continental shelf (Schmidtko et al., 2014) and increased glacial melt rates over the past decade (Pritchard et al., 2012). The thinning of floating ice shelves along most of West Antarctica, including in the Bellingshausen Sea, is one of the most dramatic signals of a changing climate (Cook & Vaughan, 2010; Paolo et al., 2015). This melting, which has been attributed to basal melt where warm ocean waters are delivered to the glaciers (Pritchard et al., 2012), is also associated with the retreat of grounding lines (Rignot et al., 2014) and the acceleration of ice sheet flow (Joughin et al., 2002). The rate of ice loss of the West Antarctic Ice Sheet (WAIS) is now estimated to be three times as large as it was in the 1990's (IMBIE, 2018). From 1989 − 2000 to 1999 − 2009 the thinning of glaciers increased by 200% (from 50 ± 14 Gt/yr to 166 ± 18 Gt/yr) and by an additional 150% from 1999 − 2009 to 2009 − 2017 (166 ± Gt/yr to 252 ± 26 Gt/yr) (Rignot et al., 2019). During the latest decade, mass loss was dominated by the Amundsen and Bellingshausen Sea sectors, contributing more than 60% of the total mass loss.

Documenting changes to those components of the ocean circulation that are responsible for basal melt is critical for accurate predictions of the future evolution of the WAIS. Yet, this remains challenging for a number of reasons. First, the circulation of the Antarctic margins depends on the large-scale flow of the Antarctic Circumpolar Current (ACC), the major polar gyres, a rich boundary current system over the continental slope (Pena-Molino et al., 2016; Thompson et al., 2018), and intricate shelf circulations steered by complex bathymetry. Furthermore, due to the lack of observations, it is difficult to ascertain changes from an uncertain baseline circulation strength and structure. The Bellingshausen Sea (BellS), the focus of this study, is at the confluence of a number of different circulation elements of varying scales and dynamics but has remained nearly unobserved.

South of the Polar Front, the penetration of warm Circumpolar Deep Water (CDW), and in particular its ability to access the Western Antarctic Peninsula (WAP) continental slope, is controlled by the boundary between the southern ACC Front and the Antarctic Slope Current (ASC) (Jacobs, 1991; Whitworth et al., 1998). The southern boundary of the ACC flows to the northeast over the continental slope along the western side of the Antarctic Peninsula (Moffat & Meredith, 2018). In the absence of major topographic barriers, warm deep water flowing onto the shelf will eventually interact with marine-terminating ice sheets and contribute to basal melting. Along the WAP, CDW flows onto the shelf nearly unrestricted, apparently largely through coherent eddies (Moffat et al., 2008; Couto et al., 2017).

Farther to the west, in the Amundsen Sea, both observational (Walker et al., 2013) and numerical (Nakayama et al., 2013) evidence exists for a westward-flowing ASC near the shelf break. This indicates that a significant reorganization of the frontal structure over the continental slope occurs in the BellS sector, where this flow is largely absent, but the processes that determine this transition have not previously been described (Thompson et al., 2020).

All ice sheets found along the coast of the BellS have experienced considerable volume loss (Paolo et al., 2015; Rignot et al., 2019) and increased basal melt in the last decades (Rignot et al., 2013, 2019). Ice shelves in the eastern BellS, including the Wilkins Ice Shelf, George VI Ice Shelf, and Stange Ice Shelf, have been documented in the past (Jenkins & Jacobs, 2008; Padman et al., 2012), but the circulation and dynamics that influence the ice shelves in the western part of the BellS are not well known. The Venable Ice Shelf, for example, is a smaller glacier by area, but has shown basal melt rates that are higher than the melt rates of any of the other ice sheets in the region (Rignot et al., 2013; Paolo et al., 2015).

The presence of warm CDW on the BellS shelf was first identified by Talbot (1988), and was explained by the absence of near-freezing, high-saline water associated with the formation of deep water masses. The exchange of CDW across the shelf break is topographically-localized at glacially-carved troughs throughout West Antarctica (Dinniman & Klinck, 2004; Moffat et al., 2008; Savidge & Amft, 2009). The BellS has two major troughs, the Belgica and Latady, located to the west and east, respectively. Within the Belgica Trough, a cyclonic circulation was inferred by Zhang et al. (2016), using data from instrumented seals and a Gade line analysis (Gade, 1979), with CDW being carried onshore along the eastern side of the trough and meltwater carried offshore along the western side of the trough. The circulation in the Latady Trough was not discussed, and this region's contribution to heat transport towards the BellS ice shelves remains unconstrained.

Coupled ice-ocean simulations carried out by Assmann et al. (2005) found the region to be dominated by a large-scale cyclonic circulation, although the model did not resolve circulation features in individual troughs. A strong coastal current formed the southern edge of this cyclonic circulation, extending from the BellS into the Amundsen Sea. The presence of a coastal current was also found by Holland et al. (2010) originating along the WAP, flowing southward into the BellS. The same study also suggests that the BellS experiences much weaker seasonal and interannual variability due to its location at the eastern edge of the Amundsen Sea low pressure system. Numerical models further suggest an important role for the exchange of water properties and tracers between the various seas of West Antarctica. In particular, Nakayama et al. (2014) suggests that basal melting in the BellS can be a driving force in the freshening of the Ross Sea, a source region of deep water formation. Model studies also show that both the Belgica and Latady Troughs are likely important for exchange between the shelf break and the ice shelves (Nakayama et al., 2017).

Comparatively little is known about the pathways and fate of the meltwater that is added to the ocean from the accelerated melting of glaciers. A freshening of the polar seas around Antarctica has been found in models as well as observations and coincides with the increased ice shelf mass loss (Schmidtko et al., 2014; Rye et al., 2014; Richardson et al., 2005; Swart & Fyfe, 2013). The vertical distribution of this meltwater in the water column and its impact on shelf and larger-scale circulation remains uncertain. Most observations suggest that the freshening has a subsurface signature, often up to several hundred meters depth, consistent with the outflow from the base of the ice shelves (Jenkins & Jacobs, 2008; Biddle et al., 2017; Loose et al., 2009; Kim, 2016). However, glacial melt can also be redistributed within the water column by mixing processes, including those related to strong hydrographic fronts that develop at the ice shelf face (Naveira-Garabato et al., 2017). The depth and density classes over which glacial melt is found in the BellS suggest an important role for meltwater as a buoyancy driving mechanism of an overturning circulation (Savidge & Amft, 2009; Moffat et al., 2008; Ruan et al., 2020).

In austral summer 2018 – 19 the TABASCO[1] (NBP19-01) research cruise set out with the goal to observe the evolution of the ASC and to describe the circulation and shelf properties of the BellS. These hydrographic and velocity observations allow us to provide the first observational estimates of heat and meltwater fluxes in this region. As is shown below, the magnitudes are comparable to those in the better-studied Amundsen Sea. During the TABASCO cruise 56 CTD stations were occupied, and two gliders were deployed in the Bellingshausen Sea (**Figure 1**), which are used in this study to describe the circulation on the shelf and its possible connections to the ASC. Data and methods are introduced in Section 2; water mass properties, velocities, meltwater fractions and heat transports on the shelf are analyzed in Section 3. Section 4 discusses these results in the context of numerical solutions of regional shelf circulation, and a summary is presented in Section 5.

2 Data and Methods

2.1 NBP1901 Cruise data

We present observations collected aboard the R/V Nathaniel B. Palmer as part of the TABASCO (NBP19-01) research cruise in December 2018 – January 2019. During the cruise, 56 temperature and salinity (CTD) profiles were collected in the Bellingshausen Sea between 27 December, 2018 and 8 January, 2019. The stations were organized into a series of transects, two of which spanned the continental slope and shelf break with the remainder located over the continental shelf (**Figure 1**). Water samples were collected at each station, and the salinity was calibrated using a Guildline PortaSal 8410A. Velocity measurements were collected at each station using a RDI Workhorse Sentinel downward-looking Lowered Acoustic Doppler Current profiler (LADCP). The LADCP was configured to record velocity in 8 m bins and processing involved the use of both the hydrographic data and shipboard ADCP data, following Thurnherr et al. (2010). CTD data was acquired using a SBE-11+ (V2) deck unit, two SBE3plus temperature sensors (accuracy 0.001°C), two SBE4C conductivity sensors (accuracy 0.0003 S m^{-1}), and two SBE43 dissolved oxygen sensors (accuracy of 2% of saturation). All data were processed following the guidelines laid out in McTaggart et al. (2010). The hydrographic data is used to analyze the temperature and density distributions, as well as to calculate meltwater fractions contained in the water column. We calculate the geostrophic velocities, which are referenced to the de-tided LADCP data. Details of data processing are provided in the TABASCO project cruise report (https://gps.caltech.edu/ andrewt/publications/TABASCO.pdf).

In addition to the ship-based measurements, two ocean gliders, Seagliders, were deployed during the cruise. The first glider (SG621) was deployed on 27 December, 2018, offshore of the shelf break near Peter I Island (67.95°S, 52.88°W). We attempted to sample the continental slope and shelf break with this glider, but with limited success due to sea ice extent. Throughout its deployment, this glider sampled within the marginal ice zone, including some narrow filaments of open water surrounded by sea ice; these observations

[1] Transport of the Antarctic Peninsula & Bellingshausen Sea: Antarctic Slope Current Origins

will be reported in a subsequent study. The second glider (SG539) was deployed just offshore of the shelf break near Marguerite Trough on 19 January, 2019. After briefly sampling the mouth of Marguerite Trough, this glider moved south and sampled across the mouth of the Latady Trough. In this study, we make use of the last 106 dives collected by SG539 (**Figure 1**). The glider completed V-shaped dives to a depth of 1000 m or to within 15 m of the seafloor, if shallower than 1000 m. Surfacing locations were separated by roughly 4 km, and as little as 1 km when the glider was over the continental shelf. While diving, the glider collected measurements of temperature and salinity with a Seabird CTSail every 5 seconds, or roughly every 1 m. Measurements were then averaged in 10 m bins (www.byqueste.com/toolbox.html). Due to problems with the compass, no depth-averaged velocities were obtained. Due to the barotropic nature of the currents in this region (shown below) non-referenced geostrophic velocities are of limited use in calculating fluxes across the glider section.

2.2 Velocity corrections and transports

The LADCP data presented in this study was de-tided using tidal velocity output from the Circum-Antarctic Tidal Simulation (CATS2008), a high-resolution inverse model based on a uniform grid size of 4 km that includes cavities under the floating ice shelves (Padman et al., 2002). The model predicts tidal effects including surface heights, tidal current velocities and transports. In order to remove the tidal effects from the LADCP data, only the tidal current velocities in meridional and zonal direction are required. We used the predicted CATS2008 tidal velocities for S2 and M2 tides (in 10 minute intervals) averaged for each station, and removed them from the original LADCP data by subtraction. The tidal velocities in the BellS were relatively small (less than 5 cm s^{-1}), and did not qualitatively impact the LADCP data (**Figure A1**).

The combined use of the CTD and LADCP data allows for the calculation of geostrophic velocities. Geostrophic velocities are calculated from the hydrography for each station pair and referenced to the LADCP data. The LADCP data is averaged and rotated to be along/across each station pair. The geostrophic velocities are then referenced to the rotated LADCP data using a least square fit. The resulting velocities are used to calculate the total transports of water and heat. While volume transports can be calculated from the LADCP data alone, this only provides a snapshot of the velocity field. Volume transports calculated from LADCP-referenced geostrophic velocities are more likely to provide a synoptic view, at least for the baroclinic component of the flow. We use the referenced geostrophic velocities for the heat transport calculations.
The heat transport Q_h was calculated at each station as:

$$Q_h = \rho C_p \int \int v\,(\theta - \theta_f)\;\mathrm{d}x\,\mathrm{d}z, \tag{1}$$

where C_p is the specific heat capacity of sea water, calculated for each profile, ρ is the neutral density of each profile, θ is the measured potential temperature, θ_f is the freezing point temperature (a function of both salinity and pressure), v is the velocity perpendicular to the section, and the integrals are taken in the vertical over the depth of the profile (dz) and in the horizontal along the section (dx).

The heat content of the CDW layer is calculated as:

$$Q_l = C_p \int_{z_{-H}}^{z_{\theta=1.1^{\mathrm{o}}C}} \rho\,\theta\,\mathrm{d}z \tag{2}$$

where C_p is the specific heat capacity of sea water, calculated for the CDW layer. The CDW layer is defined as temperatures that are warmer than 1.1°C. ρ is the neutral density of the CDW layer and θ the measured potential temperature of the same layer. This is calculated for each profile and then integrated over the depth of the CDW layer (z_{-H} $- z_{\theta=1.1^oC}$.

2.3 Meltwater calculations

Meltwater fractions are calculated using the Gade line analysis (Gade, 1979), also discussed in Jenkins & Jacobs (2008) and Biddle et al. (2017). The approach relies on the end members of three water masses that dominate shelf properties: the subsurface temperature maximum of Circumpolar Deep Water (CDW), the subsurface temperature minimum of Winter Water (WW) and glacial meltwater (MW) (**Figure 2a**). Water properties that lie along a straight line between CDW and WW end members are assumed to have 0% meltwater, although we acknowledge that end member properties can be influenced by either local or remote mixing of distinct properties; the reader is referred to Biddle et al. (2017) for a detailed discussion of these issues. The introduction of MW leads to fresher properties with a maximum meltwater fraction determined by the intersection of the MW-CDW mixing line with the freezing line (**Figure 2b**). In general, water properties are a combination of all three end members, CDW, WW and MW. This analysis breaks down near the surface where Antarctic Surface Water (AASW) is strongly influenced by surface heat and freshwater fluxes.

The properties of the MW endpoint applied in this analysis, $S = 0$ and $\theta = -89°$C, are based on Jenkins & Jacobs (2008). The properties of CDW and WW endpoints, on the other hand, are determined individually for each profile, ensuring that the meltwater fractions only involve waters between the local maximum (CDW) and minimum (WW) potential temperatures at each station. A limitation of this approach is that local WW and CDW properties may be influenced by MW, and therefore our approach tends to underestimate MW content. Applying shelf-averaged properties for WW and CDW end members did not significantly modify the patterns or spatial distribution of glacial meltwater (not shown), which is consistent with Biddle et al. (2017).

3 Results

3.1 Water mass distribution

Water masses over the Bellingshausen Sea continental shelf are distributed in a two-layer configuration (**Figure 2a** and **Figure 3**). The upper layer contains Antarctic Surface Water (AASW, $\gamma^n < \gamma^n_{\theta_{min}}$) and Winter Water (WW, $\theta = \theta_{min}$; Mosby (1934)). The lower layer consists of Modified Circumpolar Deep Water present in several degrees of modification (MCDW, 28.00 $> \gamma^n >$ 28.27, $\theta <$ 1.5°C; Whitworth et al. (1998)). The permanent pycnocline separates WW from MCDW. In this section, we refer explicitly to MCDW and identify the various temperature and salinity properties found over the shelf. However, in the other sections of this manuscript, we refer to all warm subsurface shelf water as CDW, for simplicity.

The warmest (least modified) MCDW ($\theta >$ 1.4°C) is found at the shelf break, at the eastern side of the Latady Trough (300 m – 400 m deep) (**Figure 3a**). MCDW of $\theta >$ 1.2°C is found over the entire Latady Trough, and over the eastern side of the Belgica Trough. The local temperature maximum is generally found ≈ 200 m above the bottom (trough depth 650 m), indicating offshore MCDW flows topographically unconstrained onto the shelf. Above MCDW, AASW and WW occupy the upper 200 m in the Belgica Trough and Latady Trough. While WW on the eastern side of the Latady Trough is capped by relatively warm AASW (≈ -0.4°C), surface waters over the rest of the continental shelf were relatively cold (< -1.4°C) during the TABASCO occupation. The temperature minimum of the WW lies between 50 m and 100 m. There is tilting of the permanent pycnocline across the Belgica Trough (about 300 m deep at the western side of the trough vs. 100 m deep at the eastern side) that would be in agreement with a cyclonic, baroclinic circulation inside Belgica Trough. The permanent pycnocline shows a doming structure in the Belgica and Latady Troughs in the mid-shelf transect (**Figure 3b**), indicating a general clockwise or cyclonic circulation inside these troughs.

An analysis of the temperature/salinity properties at the MCDW core (**Figure 4)** provides insight into the circulation of the Belgica and Latady Troughs. Less Modified CDW properties are observed over the eastern side of the Latady Trough (dark brown stations in panel **d**), extending southwards along $\sim$ 80°W (light brown stations in panels **c, d**). The relatively colder MCDW over the mid-shelf Latady Trough (green stations in panel **c**) suggest upstream modification takes place before this water is directed back offshore along the ridge that separates Latady and Belgica Troughs. The coldest MCDW (1.25°C, dark green in panel **d**) is found at the shelf break, at the westernmost edge of the Latady Trough, concluding the clockwise circulation inside Latady Trough.

In Belgica Trough, relatively warm MCDW is found at the center of the Trough (1.30°C; light brown stations in panel **a**). MCDW with particularly elevated θ and S values, corresponding to direct offshore CDW intrusions, are found over the eastern side of the Belgica Trough (dark brown stations in panel **b**). This less-modified MCDW encounters the more-modified MCDW, overflowing from the Latady Trough (green, in panels **a, c**), on its way onshore. Closer to the coast, strong modifications occur near the Venable Ice Shelf (magenta stations in panel **a**), giving rise to a colder and fresher version of MCDW that preserves these characteristics as it flows away from the ice shelf and back towards the shelf break along the western side of the trough (blue stations in panel **a**).

Winter water properties also show interesting modifications (**Figure 5**). In Latady Trough, the WW Θ_{min} is most eroded at the shelf break (panel **d**). Colder WW (-1.8°C) is found inside Latady Trough, and over the western side of Belgica Trough (panels **b, c**). The coldest and saltiest WW, close to freezing point (-1.85°C), is found at the western side of Belgica trough (blue stations, panel **a**). The high salinity of these waters with respect to WW measured upstream close to Venable Ice Shelf (magenta stations, panel **a**) suggests the influence of local sea ice formation processes. Influence in salinity from MCDW is, in principle, ruled out because these stations present similar θ-S properties in MCDW (**Figure 2a**).

3.2 Velocities

The temperature and salinity distributions presented in section 3.1 are complemented by information about the circulation gained from the LADCP measurements. Together, these show a consistent picture of warmer CDW flowing onto the continental shelf and towards the BellS ice shelves in both the Belgica and Latady Troughs and an offshore flow of the colder modified waters.

A striking feature of the circulation is its strong barotropic character, especially near the continental shelf break. The shelf-break section across the Belgica Trough (**Figure 6a**) indicates that the core of warmest water is associated with an onshore flow peaking of nearly 15 cm s^{-1} (St 17 – 20). The onshore flow is strongest in the center of the Belgica Trough, which is collocated with the maximum depth of the trough. The onshore flow is sandwiched between two strong cores of offshore flow. To the east, there is a strong ($>$ 15 cm s^{-1}) flow found over the eastern slope of the Belgica Trough (St 20 – 22). This outflow is associated with a lateral gradient in temperature at $\sim$ 400 m depth, suggesting that the outflow originates from the Latady Trough. The complicated and shallow bathymetry near the boundary between the mouths of the Belgica and Latady Troughs likely focuses and strengthens the outflow here. On the western side of the Belgica Trough (St 11 – 17), there is a net outflow that is weaker as compared to the eastern side, yet is also confined to narrow boundary currents.

Unfortunately, the measurements collected by the glider at the mouth of the Latady Trough did not include accurate depth-averaged currents. Due to the barotropic nature of the flow, it is difficult to infer the circulation here. However, from hydrographic properties, there is an indication of onshore flow at the very eastern edge of the Latady Trough, which could be due to flow across the shelf break or due to a southern extension of the ACC across the shelf break.

The mid-shelf section that spans the Belgica and Latady Troughs, (**Figure 6b**), indicates that the flow is weaker than at the shelf break, with all observed velocities less than 10 cm s^{-1}. Across this mid-shelf section, the flow is organized into a single region of inflow and outflow in each trough. In both troughs, the inflow is confined to the eastern side and the outflow is located on the western side, consistent with the cyclonic circulation inferred by Zhang et al. (2016). The velocity structure in the Latady Trough has a more baroclinic structure than in the Belgica Trough, with stronger flows occurring below $\sim$ 300 m depth.

A near-shore hydrographic section was collected at the face of the Venable Ice Shelf, consisting of four stations. The depth-averaged flow from these stations shows a strong offshore velocity moving away from the ice shelf along the topographic saddle separating the Eltanin Basin to the east and a deeper basin to the west in front of Venable Ice Shelf (**Figure 6c**).

Due to the barotropic nature of the flow in the troughs, referencing geostrophic velocities to either the Shipboard ADCP or Lowered ADCP data is essential for estimating the magnitude of the geostrophic transport. One difference between the geostrophic velocities and the velocities derived from the LADCP is that the onshore flow is bottom-intensified in the latter (**Figure A2b,c**). The referenced geostrophic velocities also show less structure on the western side of the Belgica Trough, such that all of the flow is offshore to the west of the maximum trough depth. The regions of narrow onshore and offshore flow in the LADCP data may indicate a coherent eddy or may be related to temporal variability that largely influences the barotropic component of the flow.

In the following sections we show that the picture of coherent cyclonic circulations that are steered by and confined within the BellS two major troughs is also consistent with meltwater and heat transport distributions, suggesting that these circulations are supported by water mass transformation processes in the southern BellS.

3.3 Meltwater Distributions

Meltwater fractions over the continental shelf are summarized in **Figure 7** and MW fractions along the two sections across the contiental slope are shown in **Figure 8**. To emphasize the MW's contribution to water mass transformation, the ordinate is changed from depth to neutral density. Notably, all stations over the continental shelf are diagnosed as having higher MW concentrations as compared to stations located over the continental slope, except for those stations located shoreward of the 2000 m isobath on the western side of the BellS (**Figure 8a**).

For all CTD stations over the continental shelf, the $\gamma^n = 28.05$ kg m^{-3} neutral density surface, found roughly at 400 m depth, marks a sharp transition in MW fraction, with MW found almost exclusively above this boundary. The absence of MW in denser density classes is in part enforced by our methodology (section 2.3), since the θ_{max} of each profile is assumed to be a pure end-member with no MW (Jenkins & Jacobs, 2008), but this transition still exists when using a shelf-wide definition of the CDW end member (not shown).

The largest MW fractions, peaking at 6 g kg^{-1}, are confined to the western edge of the Belgica Trough, found in both the shelf-break and mid-shelf sections (**Figure 7a**: St 11

– 12, **Figure 7d**: St 32 – 33). A second peak in MW is found at St 30 along the mid-shelf section in the Belgica Trough (**Figure 7e**), suggesting a flow of fresher water away from the coast both to the east and to the west of the shallow bathymetry located at 84°W, 72.5°S. At the mid-shelf section, the largest MW fractions are found between $\gamma^n = 27.85$ and 28.0 kg m^{-3} (at a depth of ~ 250 m). Peak concentrations are found on slightly lighter density surfaces ($\gamma^n = 27.87$ kg m^{-3}) at the shelf break as compared to the mid-shelf section ($\gamma^n = 27.95$ kg m^{-3}). In general, MW fractions are lower on the eastern side of the Belgica Trough. This MW distribution is consistent with an onshore flow of warm CDW, flowing towards the coast along the eastern edge of the Belgica Trough, transforming into a glacially-modified version of CDW and flowing back towards the shelf break along the western side of the trough. Thus there is both a lateral cyclonic circulation and an overturning in density space.

An elevated MW fraction signal (4 g kg^{-1}) is found in a single cast on the eastern edge of the Belgica Trough (**Figure 7a**, St. 21), and on a denser isopycnal as compared to the western side ($\gamma^n = 28$ kg m^{-3} vs. $\gamma^n = 27.85$ kg m^{-3}). This station coincides with the outflow of modified water leaving the Latady Trough (section 3.2). The glider section across the mouth of the Latady Trough also generally shows enhanced MW fractions on the western side (**Figure 7a**), including a strong positive MW anomaly near 300 km. The location of this anomaly is associated with a shallow sill that may focus the outflow here. In contrast, the region of CDW inflow in both the Belgica Trough (St. 17 – 20) and along the eastern side of the Latady Trough (St. 47 – 50) all have MW fractions less than 2 g kg^{-1}.

The short meridional section on the eastern side of the Latady Trough (**Figure 7d**) is of note because the MW fractions increase moving onshore. Furthermore, stations near the shelf break here show low amounts of MW and warmer temperatures. Despite evidence of a cyclonic circulation in the Latady Trough and little MW found at the shelf break, a MW fraction of over 3 g kg^{-1} is found on the eastern side of the trough along the mid-shelf section (**Figure 7e**, St 44 – 46). The core of this MW anomaly is on shallower density surfaces, $\gamma^n \approx 27.85$, than in the Belgica Trough. This enhanced MW concentration flowing towards the George VI ice shelf may indicate a southward extension of meltwater, derived from glacial run-off along the WAP, that has collected within the Antarctic Peninsula Coastal Current (APCC) and is delivered into the BellS (Moffat & Meredith, 2018).

A significant amount of MW (3 g kg^{-1}) is found across the meridional secrtion separating the Belgica and Latady Troughs (**Figure 7c**). Together with the depth-averaged velocities at this station (**Figure 6**), this suggests an exchange of water properties between the two troughs that brings elevated MW fractions into the Belgica Trough where it joins the onshore flow. This may lead to higher meltwater fractions in the Belgica Trough and contribute to the modification of water properties that are flowing southward before they reach the coast. While the MW exiting the Latady Trough is found in shallower density classes than the on-shore moving CDW, the flow is largely barotropic and so may carry this MW back towards the coast leading to multiple modification events before leaving the BellS.

Finally, near the Venable Ice Shelf front, the peak MW concentration is found between the $\gamma^n = 27.95$ and 28.00 kg m^{-3} density surfaces, which corresponds to a depth of roughly 400 m (**Figure 7b**). The subsurface peak in MW is consistent with an outflow from the ice shelf cavity beneath the Venable Ice Shelf; the draft of the ice shelf is estimated to have an average depth of 280 m (Morlighem et al., 2019). This is the deepest isopycnal on which large MW fractions are found, suggesting that the MW core both shoals and becomes progressively lighter as it moves towards the shelf break (Zhang et al., 2016).

The combination of ice shelf melt and the topographically-steered circulation over the shelf leads to a dramatic difference in MW fractions over the continental slope on the western and eastern extent of the BellS (**Figure 8**). The outflow of MW, accumulated broadly over the continental shelf of the BellS and potentially after interactions with multiple ice shelves, is focused at the western edge of the Belgica Trough (**Figure 8a**), with MW fractions of 6 g kg^{-1} – nearly five times larger than the values found on the eastern side of the BellS (**Figure 8b**). The elevated MW fraction is found in water as deep as 2000 m over the continental shelf, establishing a sharp front in MW, associated with the southern boundary of the ACC. The negative anomaly in MW fraction found at St. 8 is likely evidence of a mesoscale eddy or filament advecting offshore water shoreward over the slope. The large MW fractions found at the western extent of the Belgica Trough are consistent with the meltwater distribution inferred from coarser hydrographic profiles from instrumented seals by (Zhang et al., 2016) and may indicate that this region is the primary export site from the BellS.

Both the MW concentration and the vertical extent of the density classes that host this freshwater contribute to the total MW content. The MW distribution over the shelf (**Figure 9**) is largely consistent with the hydrographic sections discussed above. The area in front of Venables Ice Shelf show the largest values, increasing towards the coast to 2.9 m of meltwater. MW content across the shelf-break and mid-shelf sections in both the Belgica and Latady Troughs are lower with around 0.9 – 1.3 m of meltwater. Strikingly, the MW content increases again at the shelf break in a narrow band of isobaths between 1000 and 2000 m. Here we find as much as 2.3 m of meltwater in a much thicker (about 350 – 450 m) layer. The elevated MW content here suggests that MW distributed broadly over the continental shelf is collected as the western edge of the BellS and delivered westward via the circulation over the continental slope.

3.4 Volume and heat transports

Volume and heat transports were calculated at the mouth of the Belgica Trough and at the mid-shelf section occupying the Belgica and Latady Troughs (**Figure 10**). A total of 6 Sv enter the Belgica Trough through the deepest part of the trough (**Figure 10a** middle panel, St 16 – 19), and a total of 6.6 Sv flow offshore over the rest of the section. The largest offshore transports are found close to the gap connecting Belgica to Latady Trough (3.6 Sv at St 20 – 22). The net transport across the mouth of the Belgica Trough is nearly closed (0.6 Sv net offshore transport).

Transports at the mid-shelf section are generally weaker than those at the shelf break section. A weak onshore flow of 0.6 Sv was measured at the deep station-pairs of the Latady Trough (**Figure 10b**, middle panel, St 44 – 46), suggesting we are likely missing a narrow onshore current on the eastern side of the trough. As can be seen in the bathymetric profile (**Figure 10b**, top panel), the mid-shelf section was not properly closed; thick sea ice prevented the ship from closing the section across the Latady Trough. The offshore flow on the western side of the Latady trough was of 1.6 Sv (**Figure 10b**, middle panel). Roughly 2 Sv flow back onshore along the eastern side of the Belgica Trough, but only 0.6 Sv of transport flow back towards the shelf break on the western side of the trough. Such weak offshore flow measured on the western side of the Belgica Trough may indicate that a substantial part of water flows back towards the shelfbreak over the westernmost BellS continental shelf (not sampled here).

Integrating volume transport across both troughs (**Figure 10b**, middle panel), results in a net onshore transport of 1.3 Sv. This discrepancy may arise from not completely closing the Latady Trough, therefore missing a topographically steered circulation on the eastern side of Latady. By excluding station 45, at which the LADCP data recorded a strong southward flow, the imbalance is reduced to only 0.4 Sv (**Figure 10b)**, broken line). Alternatively, the 1.3 Sv (onshore) imbalance could indicate that we are indeed missing a more distributed flow of water moving back towards the shelf break over the western shelf of the BellS.

The spatial distribution of heat fluxes follows a similar pattern. The largest magnitude heat transport occurs at the eastern side of the Belgica Trough (**Figure 10a**). In the Belgica Trough, a total of 0.9 TW enter along the bottom of the trough (stations 17 – 19). The heat transport balances to +0.1 TW. At the mid-shelf section across the Belgica and Latady Troughs (**Figure 10c**), 0.5 TW enter along the eastern side of the Belgica Trough. About 70% of the offshore heat transport (0.3 TW) takes place along the western side of the Latady Trough (St 42 – 44). The net heat transport across the mid-shelf section of Latady and Belgica troughs, towards the ice shelves is 0.3 TW.

The thickness and heat content of the CDW layer at each station provide additional information about the locations where the heat is transported onto the shelf and lost through a combination of interactions with ice shelf meltwater or via surface cooling. To estimate the thickness of the CDW layer we use a temperature threshold of 1.1°C (**Figure 11**). The thickness and heat content of the CDW layer is largest at the mouth of the Belgica Trough and at the eastern side of the Latady Trough. In the Latady Trough, the CDW thickness remains fairly constant (∼325 m), but its heat content presents a zonal gradient, with more heat content on the eastern side of the trough. This suggests there is significant meltwater contribution from the BellS ice shelves in Latady Trough that supports modification of CDW along its path towards shelf break.

At the connection between the two troughs, the CDW layer is thinner (∼ 100 – 150 m) and the heat content is lower (0.6 GJ m^{-2}) than at the mouth of the Belgica Trough (1.5 GJ m^{-2}). This confirms CDW recirculates around the Latady Trough before moving offshore and into the Belgica Trough through the gap connecting the two troughs. In front of the Venable Ice Shelf, a few stations show a thick (> 150 m) yet significantly cold CDW layer. The western side of the Belgica Trough presents the thinnest CDW layer (∼ 50 – 75 m) with lowest heat content (0 – 0.2 GJ m^{-2}). This confirms the western side of the Belgica Trough as the major pathway for meltwater mixtures exiting the BellS towards the shelf break.

4 Discussion

4.1 Comparison to numerical models

The observations described above are the first to make quantitative estimates of the shelf circulation, and therefore the best point of comparison is with numerical simulations that include the regional circulation of West Antarctica. A prominent feature of the observations is the delivery of warm water towards the BellS ice shelves as well as the delivery of waters modified by glacial melt away from the shelves via narrow boundary currents that are steered by the bathymetry and have a lateral scale of ∼10 km. This puts a strong constraint on the horizontal resolution needed to accurately capture physical processes that are controlling the shelf circulation (St-Laurent et al., 2013; Stewart & Thompson, 2015). It is perhaps not surprising that early studies (e.g. Assmann et al. (2005); Holland et al. (2010)) only resolve a broad-scale cyclonic circulation that effectively spans the entire continental shelf. In particular, in Holland et al. (2010), the near-surface, two-dimensional stream function shows circulation extending from the WAP, well north of Marguerite Trough to the eastern boundary of the Amundsen Sea. At 200 m depth, their stream function shows more confinement to the Bellingshausen Sea. Holland et al. (2010) do not provide an estimate of the depth-integrated transport over the shelf, although the annual mean horizontal streamfucntion at 200 m peaks at roughly $5{\times}10^3$ m^2 s^{-1}, which assumed to be uniform over an average depth of 500 m is equal to 2.5 Sv. This value is comparable to the maximum onshore transport calculated in the Belgica and Latady Troughs (section 3.4).

More recent modeling efforts have produced higher-resolution realizations of the BellS circulation and support the spatial variability in water properties apparent in our observations. In particular, Nakayama et al. (2014), analyzing output from a simulation with non-uniform grid spacing that reduces to less than 5 km over the continental shelf, presents distinct fates for glacial MW entering from ice shelves located in the western, central and eastern parts of the BellS. Following a decade of integration, the largest MW content is confined to the Belgica Trough. This suggests (i) the importance of melt from ice selves found along the southern edge of Eltanin Bay that are directly connected to the Belgica Trough and (ii) the transfer of MW from the Latady Trough into the Belgica Trough before leaving the continental shelf. In this simulation, the MW is distributed broadly in the Belgica Trough, rather than being confined to the western edge. Indeed, the regions of largest MW content are found on the eastern side of Eltanin Bay, suggesting a pooling of MW arising from eastern ice shelves, such as George VI and Stange. While the exact position of inter-trough exchange (between Belgica and Latady) is difficult to discern from our limited observations, we do indeed see regions of enhanced flow between troughs in regions where the bathymetry is deep, for instance near stations 22 – 25 and 34 – 37 (**Figure 6c**). While our glacial MW estimates peak in the western boundary of the Belgica and Latady Troughs, we also find elevated meltwater fractions spread across the same density surfaces. Thus, both models and observations are consistent with a significant degree of re-circulation over the shelf that may trap modified waters for up to decades, and would integrate changes in forcing, such as wind forcing at the shelf break, that might be active on shorter timescales (Walker et al., 2007; Jenkins et al., 2018). Models, when tracking CDW with the help of tracers, seem to indicate a higher concentration of CDW on the eastern side of the Latady Trough. This is confirmed by our observations that show warm water in the same location.

The long-term fate of the glacial MW in Nakayama et al. (2014) is remarkable. Despite its broad distribution within the Belgica and Latady Troughs, upon delivery to the shelf break, the glacial MW predominantly flows westward; MW content is low over the continental slope of the WAP. Again, this is consistent with our observations that show large differences in MW faction on the cross-slope sections at the western and eastern edges of the BellS. Additionally, the westward pathways appears to be exclusively over the continental slope, in part due to the extremely shallow bathymetry to the north of Abbott Ice Shelf. To our knowledge, there are no ship-based observations in this region of shallow bathymetry, due to predominantly northerly winds producing packed sea ice conditions nearly year round. However, seal-based estimates of MW content was also low in this area (Zhang et al., 2016). Furthermore, experiments in which MW was only tracked from Abbott Ice Shelf showed limited distribution, confirming the relative impermeability of the shallow shelf region to lateral exchange (Nakayama et al., 2014). It remains an open question as to whether a narrow coastal current connects the southern BellS to the eastern Amundsen, perhaps even flowing under the Abbott Ice Shelf. However, even 2 km resolution models may struggle to resolve this feature. Overall, our observations have confirmed a number of features that have been simulated in high-resolution models of the BellS, and they highlight the importance of compact circulation features and topographic control on MW transport.

4.2 Comparison to the Amundsen Sea

In the Amundsen Sea, just like in the Bellingshausen Sea, basal melt is driven by CDW that enters the shelf via troughs (Webber et al., 2019; Dotto et al., 2019). The depth of the CDW in the Amundsen Sea (350 – 500 m) agrees with the depth observed in the Bellingshausen Sea. While some studies have shown the inflow of the warm water to be baroclinic (Arneborg et al., 2012; Wahlin et al., 2013) other direct velocity observations, on the other hand, show it to be barotropic (Kalen et al., 2015; Biddle et al., 2019) as observed for the Belgica Trough. The volume transport due to the flow on the shelf was found to be 1.5 Sv in the Amundsen Sea (Thurnherr et al., 2014) compared to a cumulative transport of 5 Sv towards the glaciers at our mid-shelf section. However, the net ocean heat transport in both regions are more comparable with 3.3 TW in the Amundsen Sea (Webber et al., 2019) and 0.7 TW in the Bellingshausen Sea. Furthermore, it is interesting to note, that MW is present across the entire continental shelf of the Amundsen Sea, with strong outflow at the western sides of two troughs (Biddle et al., 2019). This is consistent with our findings of MW across the entire Bellingshausen Sea shelf and export pathways along the western sides of the Belgica and Latady Troughs. One notable difference between the MW in the Amundsen and Bellingshausen is the larger amount in the former. In front of Thwaites glacier, meltwater in the water column accumulates to as much as 4.5 m, while they are a maximum of 2.9 m in the Bellingshausen Sea, infront of the Venable glacier. However, our calculation does not include the top 200 m and in some locations MW fractions in the Amundsen Sea were found to be largest in the surface layer. In addition, measurements taken infront of George VI in 1994 suggest meltwater fractions of up to 20 g kg^{-1} at around 200 m with transports of up to 0.2 Sv.

4.3 Variability of the regional circulation

This study, along with Ruan et al. (2020), provides the first hydrographic overview of the entire BellS and suggests that this region plays a key role in integrating water modification processes throughout West Antarctica. However, cautious interpretation of this data set is required due to our limited ability to assess temporal variability. On seasonal timescales, the numerical simulations of Mathiot et al. (2011) show that the frontal circulation over the shelf is susceptible to seasonal variability in the BellS, a result confirmed through observations by Armitage et al. (2018). Changes in the wind stress and wind stress curl will almost certainly modify both the properties of CDW and, perhaps more importantly, its thickness over the continental shelf, similar to variability observed in the Amundsen Sea (Dutrieux et al., 2014; Jenkins et al., 2018). Thus even comparing years when hydrographic data over the shelf is available (1994, 2007, 2019) - the focus of future work - is challenging because data were collected at different times of the year. Data collected by instrumented seals is a promising resource for analyzing interannual variability, although this is hampered by the spatial heterogeneity in how the seals forage from year-to-year, i.e. they do not often return to the same spot. Nevertheless, integrating these disparate data sets along with new remote sensing products (Armitage et al., 2018) should help to determine whether the BellS experiences similar shifts between warm and cold regimes that have been observed in the Amundsen Sea (Dutrieux et al., 2014; Jenkins et al., 2018).

Over longer timescales, however, there are features of the BellS that are distinct from the Amundsen and relevant for the evolution of the West Antarctic circulation. While the Belgica and likely the Latady Trough host an inflow of CDW focused in deep troughs, similar to the Amundsen, the eastern BellS supports the inflow of a much lighter and fresher water mass related to the southward flow of the APCC. This could influence the vertical stratification of BellS waters and impact air-sea exchange, and in particular heat loss, in the large polynyas of the BellS in ways that are distinct from the Amundsen. Furthermore, due to the shallow bathymetry to the west of the Belgica Trough, the outflow of modified waters is much more confined to the shelf break in the BellS (Thompson et al., 2020) as compared to the Amundsen (Nakayama et al., 2017). This, in turn, could play an important role in setting properties of the Antarctic Slope Current. This is particularly important as the outflow from the BellS occurs at the confluence of the ACC's southern boundary and the eastern extent of the Ross Gyre, opening the possibility of the BellS circulation responding to more remote forcing, such as the strength of the Ross Gyre. Finally, the Amundsen and BellS may also influence the structure of the Ross Gyre through the export of MW from the shelves to the open ocean, hence providing a direct link to the deep water formation (Nakayama et al., 2018).

5 Summary

Data from the 2018–2019 NBP1901 cruise is used to investigate the circulation over the continental shelf of the Bellingshausen Sea and this region's role in linking flow features throughout West Antarctica. Flow through the BellS connects the West Antarctic Peninsula (**Figure 1**), where CDW on the continental shelf is warmest, to the Amundsen Sea where changes in the temperature of CDW has been most rapid (Schmidtko et al., 2014). Thus the circulation towards and away from floating ice shelves in the BellS will be critical part of the response of the West Antarctic climate to continued warming of the Southern Ocean. Relatively little is known about mechanistic controls on the BellS circulation features, in large part because dedicated observations in this region have been rare. A combination of ship-based and glider-based hydrography, along with lowered ADCP data, has provided a shelf-wide snapshot of this circulation as well as transports of heat and meltwater.

On the BellS shelf, warm CDW is found broadly below 300 m. The warmest CDW is found on the eastern side of the Latady Trough, and this water mass cools progressively from east to west across. There are multiple lines of evidence, including velocity fields, meltwater concentrations, and heat transport estimate that this cooling is indicative of modification through interaction with one or perhaps multiple ice shelves along the coast of the BellS. The signature of these modifications is most pronounced in water flowing offshore on the western edges of the two prominent troughs. This suggests that the ice shelf interactions support cyclonic lateral circulations in both the Belgica and Latady Troughs as well as an overturning in density space. This circulation is also consistent with the flow field diagnosed from geostrophy referenced to the LADCP data as well as the meltwater distributions. While the meltwater is broadly distributed over the shelf, meltwater fractions peak, with values up to 6 g kg^{-1}, on the western edge of each trough with smaller magnitudes MW on the eastern edges.

Despite providing a snapshot of the circulation structure, the transport is nearly closed across both our shelfbreak and mid-shelf section. The cumulative transport, comparable to a horizontal streamfunction, reaches a maximum values of roughly 2 Sv in each trough, comparable to the circulation strength in the Amundsen Sea. Due to the largely barotropic nature of the flow, we infer the baroclinic circulation, more closely linked to the overturning (Wahlin et al., 2013), to be much smaller. The largest heat transport occurs at the eastern side of both troughs, with 1.7 TW moving onto the shelf while about 1 TW are leaving the area. The thickness of the CDW layer and its heat content also peak on the eastern side of each trough; the CDW layer is progressively eroded and cooled while circulating through the troughs.

While these observations improve our understanding of the BellS circulation, open questions remain. In particular, due to sea ice extent we were not able to close the eastern boundary of the Lataday Trough, and the origin of the water flowing into this trough remains unclear. Future observations are needed to assess the link between inflow to the BellS and the Antarctic Coastal Current as well as how this can influence ice-shelf melt rates (Hellmer et al., 2012; Moffat et al., 2008; Kim, 2016). The persistence of connections between the WAP (east of the BellS shelf), the BellS shelf, and the Amundsen Sea (west of the BellS) remains uncertain. Such a connection would be a crucial piece in understanding heat and meltwater transport throughout the region. Based on the large-scale cyclonic circulation over the West Antarctic shelf (Assmann et al., 2005; Holland et al., 2010), this connection would imply that processes over the BellS shelf are influenced by the dynamic Antarctic Peninsula to the east, while dynamics in the fast-changing Amundsen Sea may be influenced by upstream processes in the BellS. The latter relationship is likely considering the evidence in these observations that meltwater exported from the BellS shelf is directed into a slope current that is directed towards the Amundsen Sea.

Acknowledgments

We acknowledge essential contributions from the captain and crew of the R/V Nathaniel B. Palmer as well as the Antarctic Support Contract staff during NBP19-01. This work was supported by the National Science Foundation. AFT, XR, and MF were supported by NSF OPP-1644172 and the David and Lucille Packard Foundation. LSC, KS, NS, RS, and CL were supported by NSF OPP-1643679. RO is supported by the COMPASS project from the European Research Council under the European Union's Horizon 2020 research and innovation program (grant agreement n° 741120).

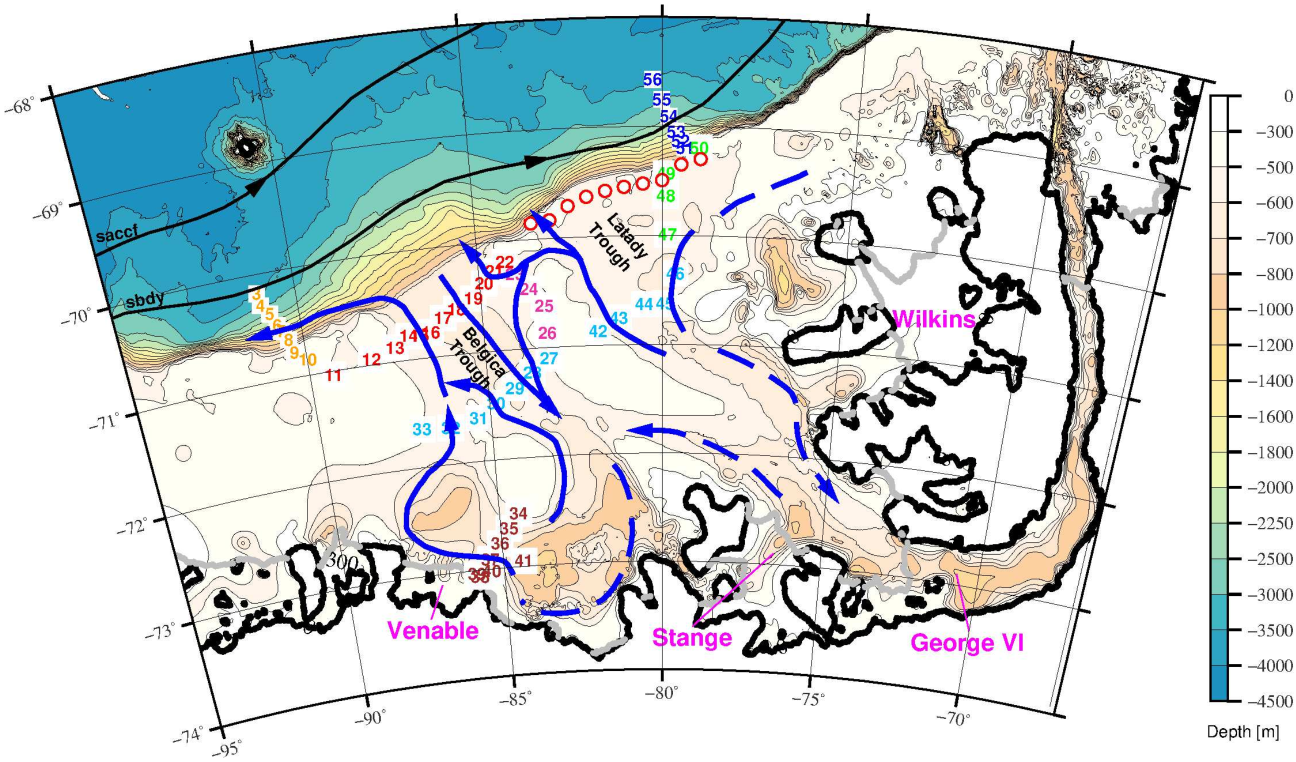

Figure 1. Bathymetry of the Bellingshausen Sea with CTD stations and a schematic of the circulation derived in this study. Bathymetry contours are shown in color (m). The black lines and arrows show the climatological positions of the southernmost fronts of the Antarctic Circumpolar Current (Orsi et al., 1999) (saccf = Southern Antarctic Circumpolar Current Front, sbdy = Southern Boundary). The coastline is indicated with a thick black line. The faces of the ice shelves are shown with a thick gray line; names of the ice shelves are given in pink. Bathymatry under the ice shelves has not been removed to provide a sense of the ice cavity shape. Conductivity-Temperature-Depth stations (number and location) are indicated in colors that are used throughout this study. The glider section is shown with red circles. A schematic of the circulation on the Bellingshausen Sea shelf is shown in blue arrows, where solid and dashed lines show, respectively, flows directly resolved by the observations and flow inferred from the property distributions over the shelf.

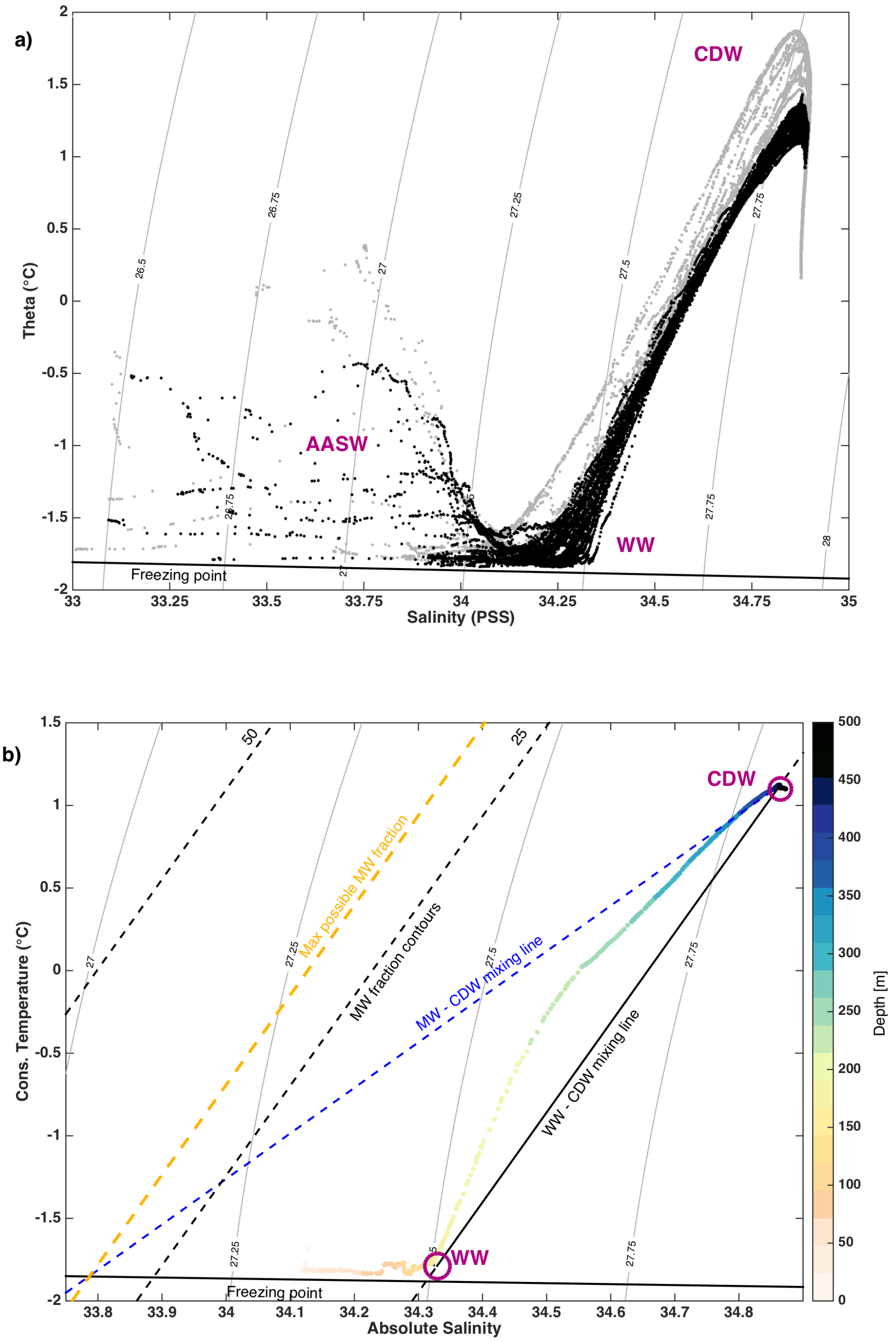

Figure 2. a) Temperature-Salinity (Θ-S) properties of all stations sampled on the BellS shelf (black) and across the slope (grey) from CTD and glider data. (b) Example of meltwater calculation for profile 11, where colored dots show the depth (m). Both a) and b) show potential density contours as well as the freezing point line (thick, black contour). Purple circles/labels show the location of the Antarctic Surface Water (AASW), Winter Water (WW) and Circumpolar Deep Water (CDW). In b) CDW and WW would mix along the solid black line. The broken blue line shows the characteristics of water that would be a mix of CDW and pure meltwater (i.e salinity of zero, θ=-89°C). Black broken lines are the meltwater fraction (g/kg). The maximum possible meltwater fraction is given by the golden, broken line, set by the intersect of the MW - CDW mixing line. The θ/S properties of station 11 shown here have a large meltwater fraction between 250 – 600 m, where the dots fall along the MW - CDW mixing line.

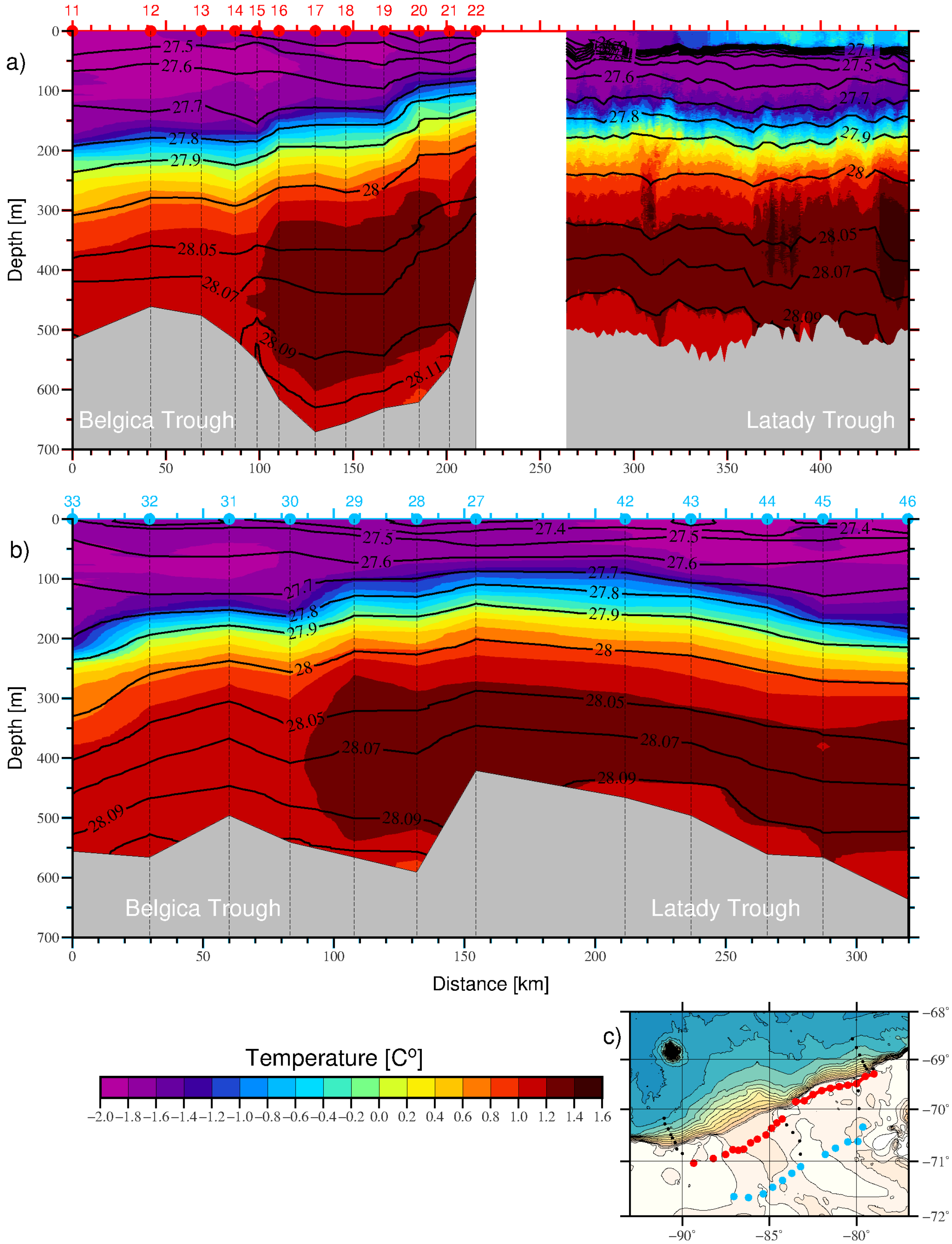

Figure 3. Potential temperature sections spanning the Belgica and Latady Trough sections. The data are plotted as distance from the westernmost station versus depth. (a) Temperature section at the shelf break in the Belgica Trough (stations 11 – 22, left) and the Latady Trough from the glider (right). Black vertical lines indicate the location of the stations. Density is shown as black contours. Positions of glider dives are not shown since that data were smoothed and gridded before displaying. (b) Mid-shelf temperature section for Belgica (stations 33 – 27) and Latady (stations 42 – 46) Troughs. (c) Map of the station positions with red and blue dots corresponding to panels (a) and (b), respectively. Station numbers can be found in Figure 1.

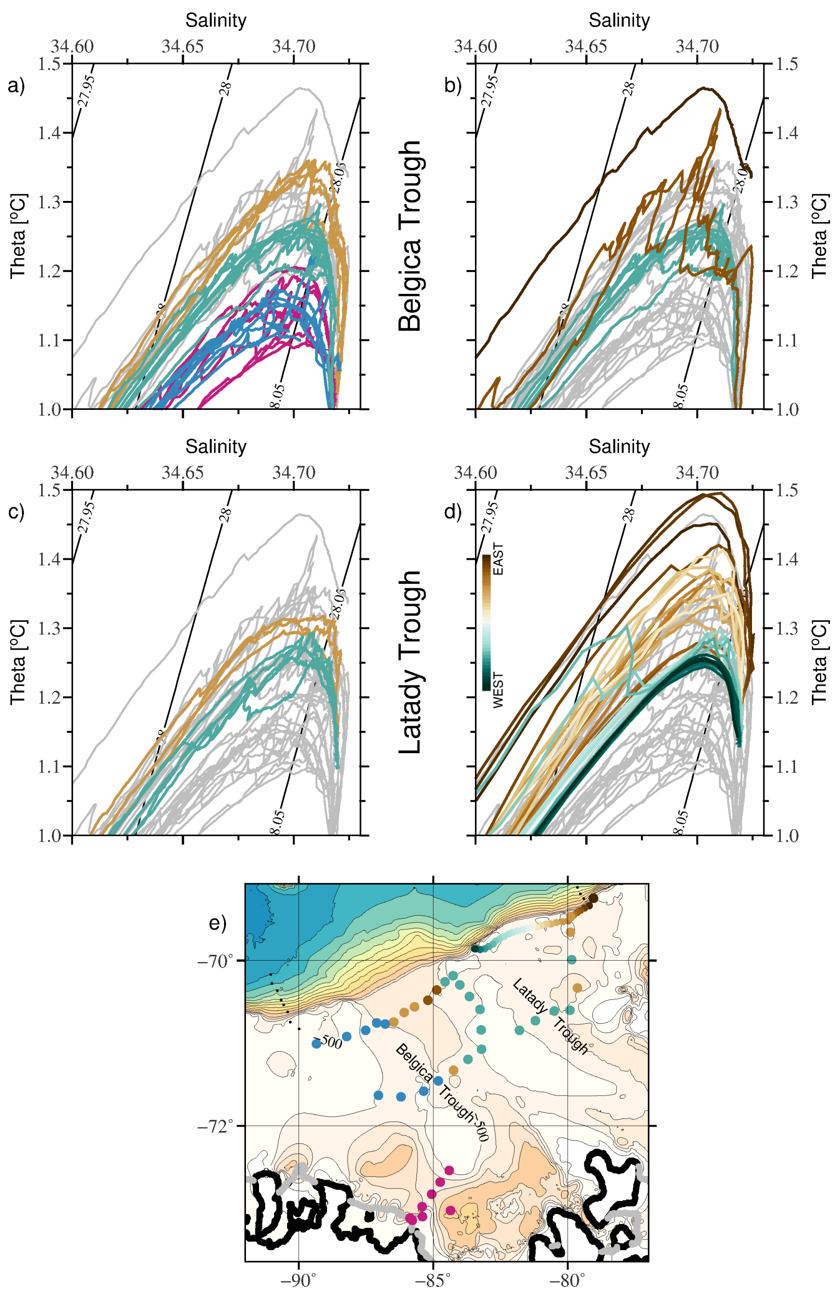

Figure 4. Temperature and salinity properties of Circumpolar Deep Water (CDW) in the (a, b) Belgica and (c, d) Latady Troughs. In each panel, the T/S properties for all shelf stations (11 – 50) are shown in gray. In (a) stations in the Belgica Trough (St. 11 – 22, 27 – 33), the connection between the two Troughs (St. 23 – 26), and in front of the Glacier (St. 34 – 41) are color coded by their respective CDW class: violet for glacially modified CDW, blue for CDW that is moving towards the shelfbreak, green for CDW modified due to re-circulation on the shelf, and light brown for CDW originating from offshore. (b) shows the same as (a) but for stations with a mixture of modified and offshore CDW. (c) shows the same as a) but for CDW in the Latady trough. (d) show the profiles obtained from the Glider, color coded showing a transition of CDW from recirculated to offshore from west to east. All stations are shown on the map (e) in the color that represents their CDW.

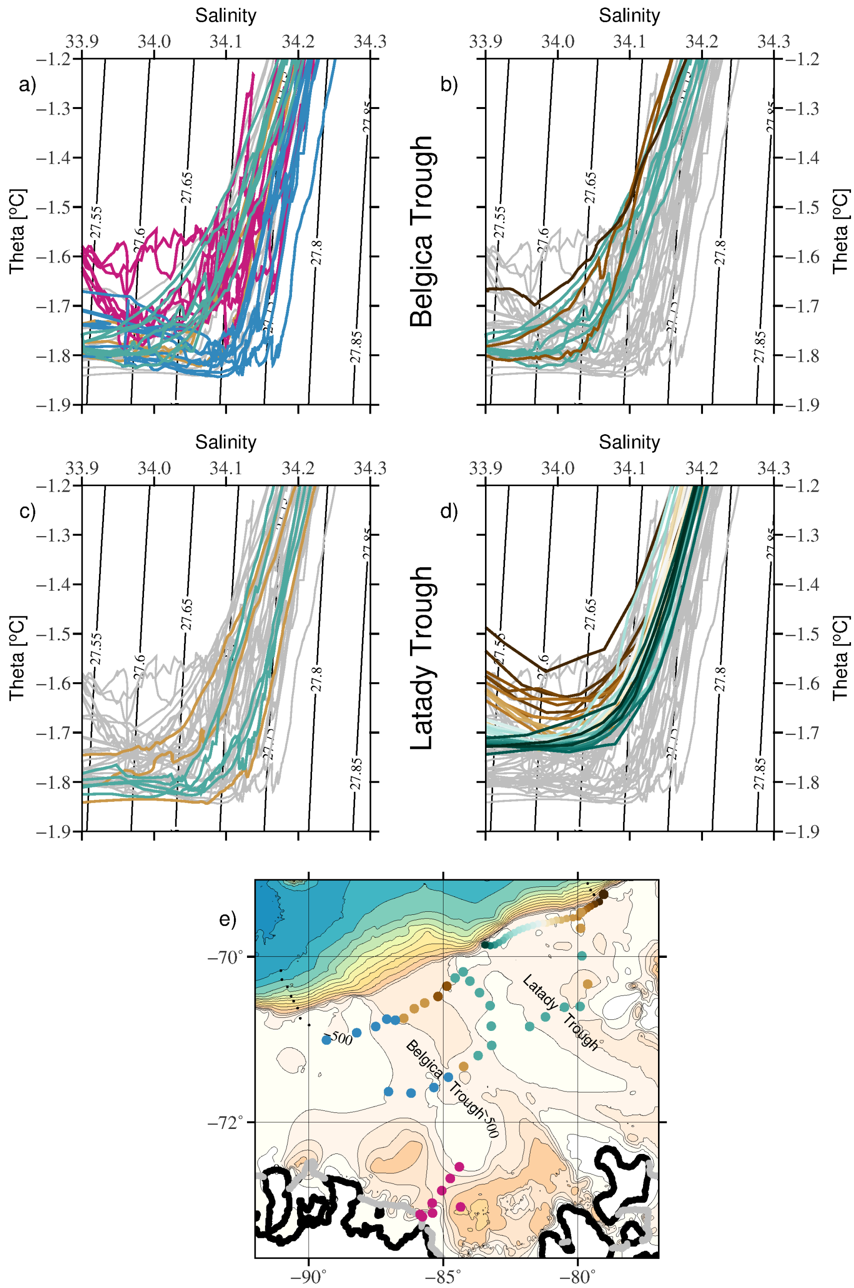

Figure 5. Same as Figure 4, but for Winter Water.

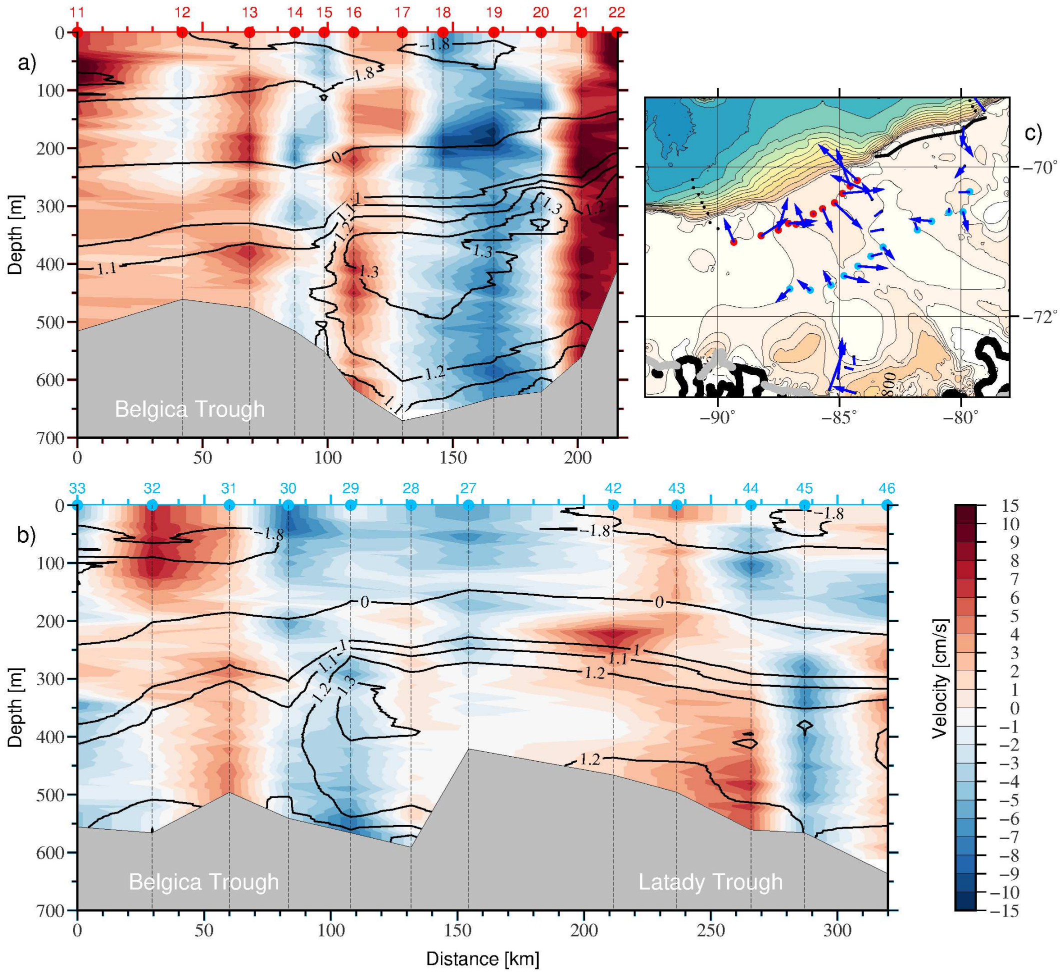

Figure 6. LADCP velocity data for (a) the Belgica trough (shelfbreak) section and (b) the Belgica and Latady Trough (mid-shelf) section. Velocity estimates from the glider are not available. Velocities (cm s^{-1}) shown in each transect are rotated to be perpendicular to the section. Positive velocities (red) are directed offshore, negative velocities (blue) are directed on to the shelf. Temperature contours are shown in black. Panel (c) shows the depth-averaged velocities at each station from the LADCP data (blue arrows).

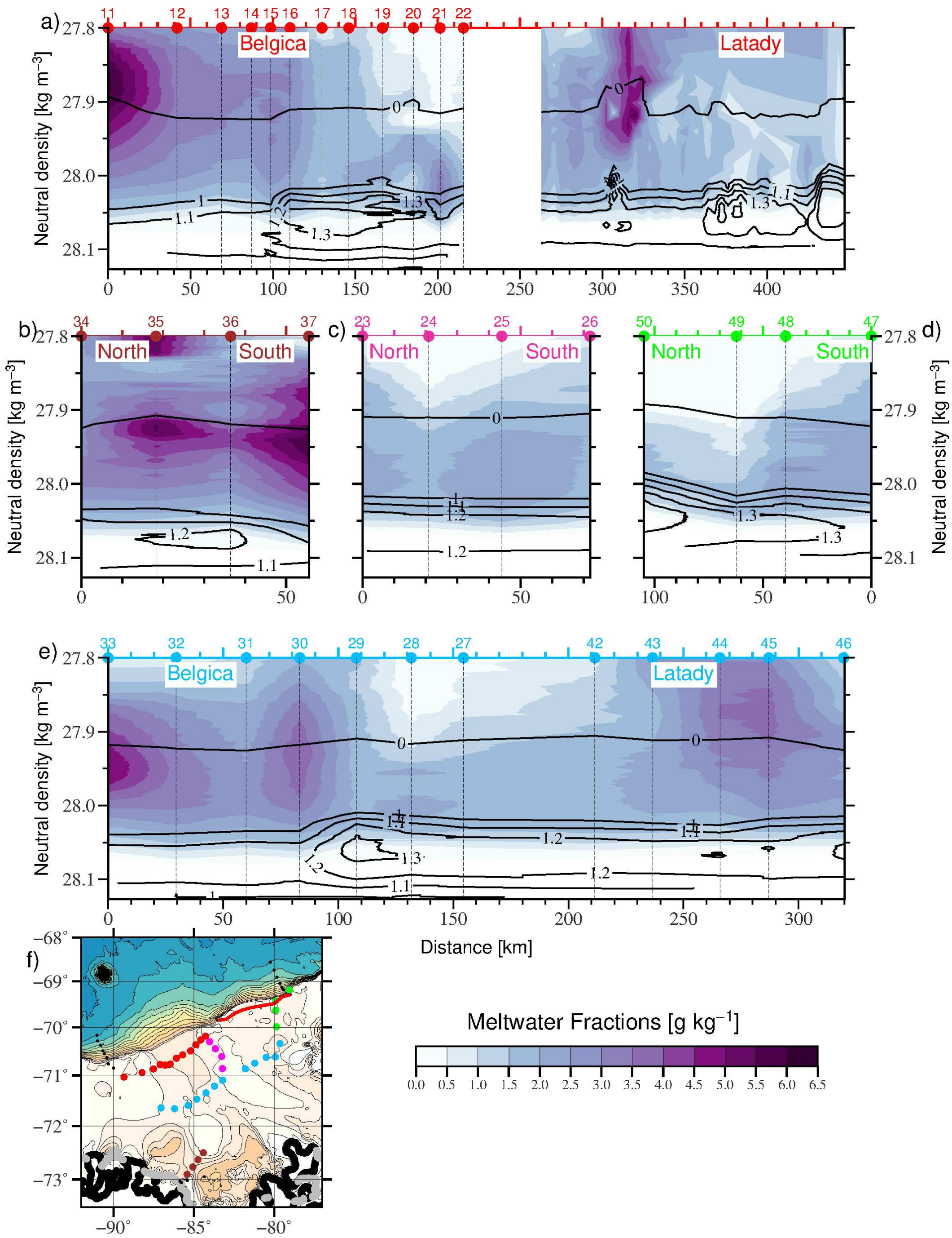

Figure 7. Meltwater fractions (g kg^{-1}, color) in the Belgica and Latady Troughs over-layed with temperature contours. The sections are shown in distance vs. density starting below 200 m. The upper 200 m are excluded from the figures to eliminate signals due to processes such as sea ice melt, rather than Glacial ice melt. The sections show distributions(a) at the shelf break across the Belgica Trough (stations 11 – 22) (left) and the Latady Trough (Glider data) (right), (b) near the Venable Ice shelf, (c) the region connecting the Belgica and Latady Troughs, (d) the eastern Latady Trough, and (e) the mid-shelf section spanning the Belgcia (stations 33 – 27) and Latady Troughs (stations 43 – 46). All stations are color coded and shown on the map in panel (f).

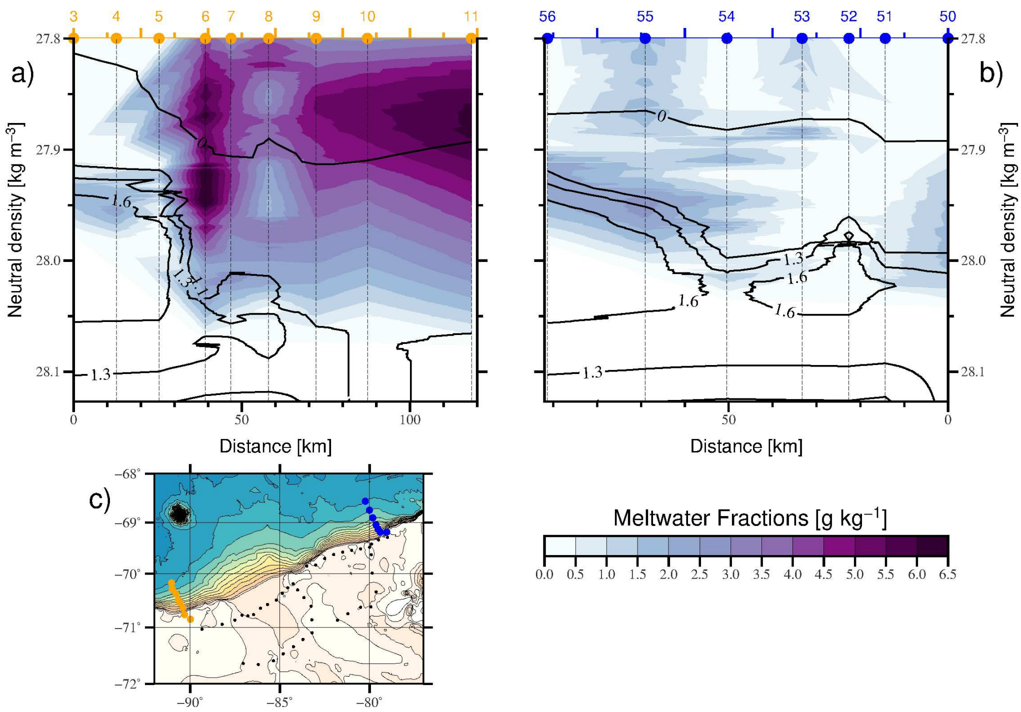

Figure 8. Meltwater fractions (g kg^{-1}, color) along the sections spanning the continental slope (a) west of the Belgica Trough and (b) east of the Latady Trough. The location of the sections is shown in the map in panel (c).

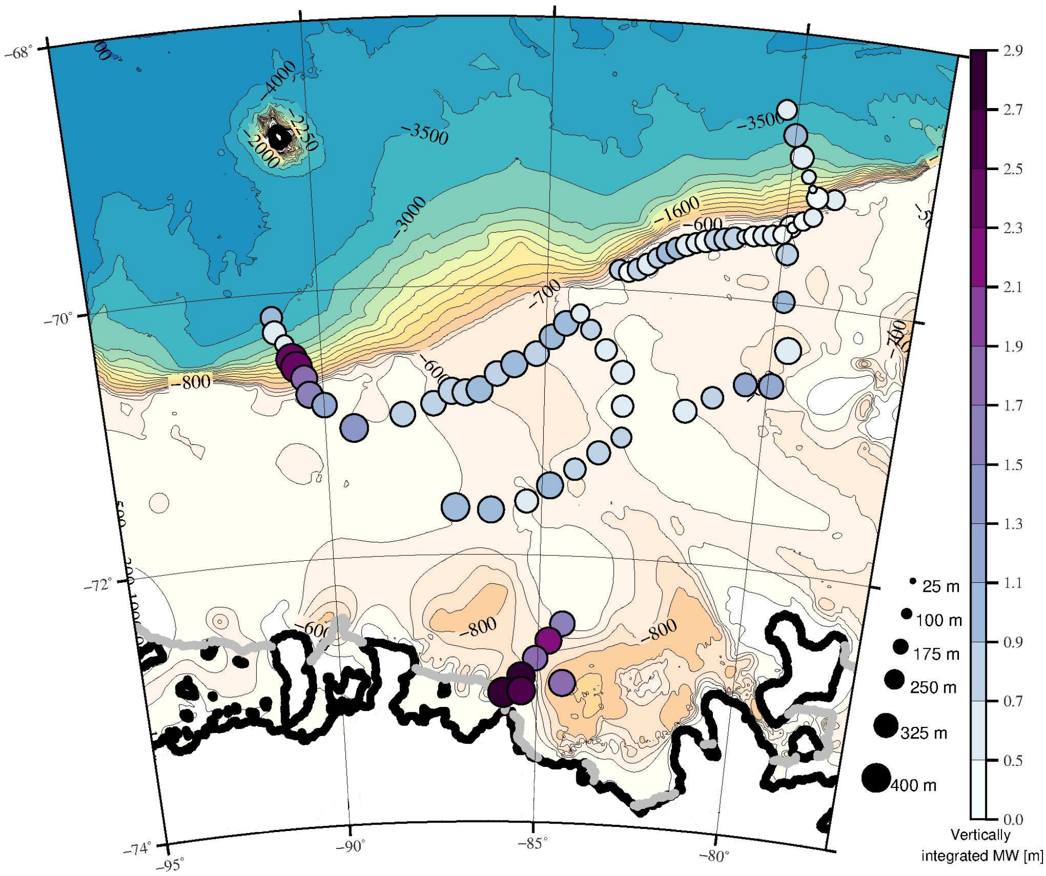

Figure 9. Map of meltwater distribution showing the thickness (m, size of circles) and vertically-integrated meltwater content (m, color) for each station. The thickness is calculated from water having a meltwater fraction greater than 1 g kg^{-1}. The bathymetry (m) is given in color as in Figure 1.

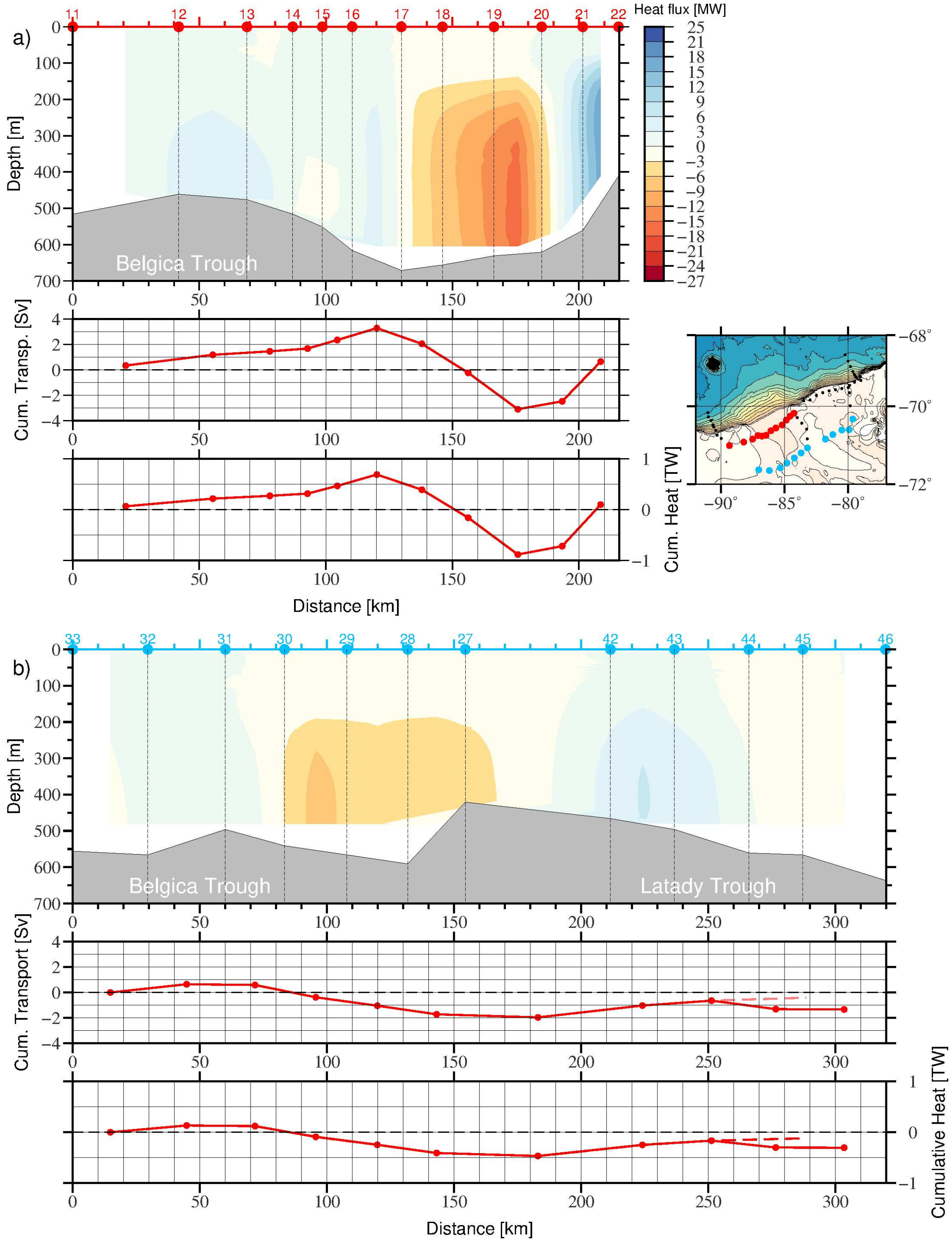

Figure 10. Transport estimates for the Belgica and Latady Troughs based on referenced geostrophic velocities. (a) Distribution of heat transport (MW) across the mouth of the Belgica Trough (color, stations 11 – 22), calculated as in equation (1). The panels below show the cumulative volume transport (Sv) and the cumulative heat flux (TW). (b) As in panel (a), but but for the mid-shelf section that span the Belgica (stations 27–33) and the Latady (stations 42 – 26) Troughs. The inset map shows the location of the sections in panels (a, red) and (b, blue).

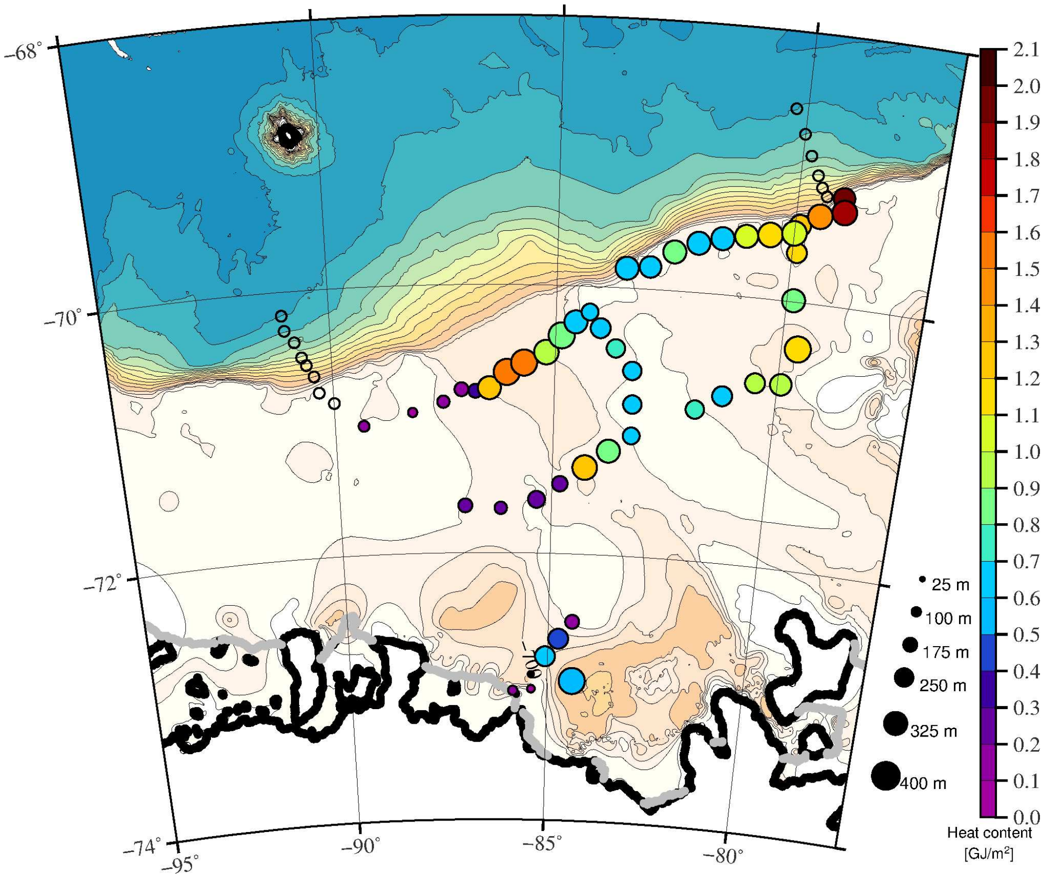

Figure 11. Map of heat distribution over the continental shelf showing this thickness of the CDW layer (m, size of circles) and the heat content (GJ m^{-2}, color) for each station. The CDW layer is defined as the part of the water column where temperatures exceed 1.1°C. The heat content of this layer is calculated using equation (2).

679 ## Appendix A Additional figures

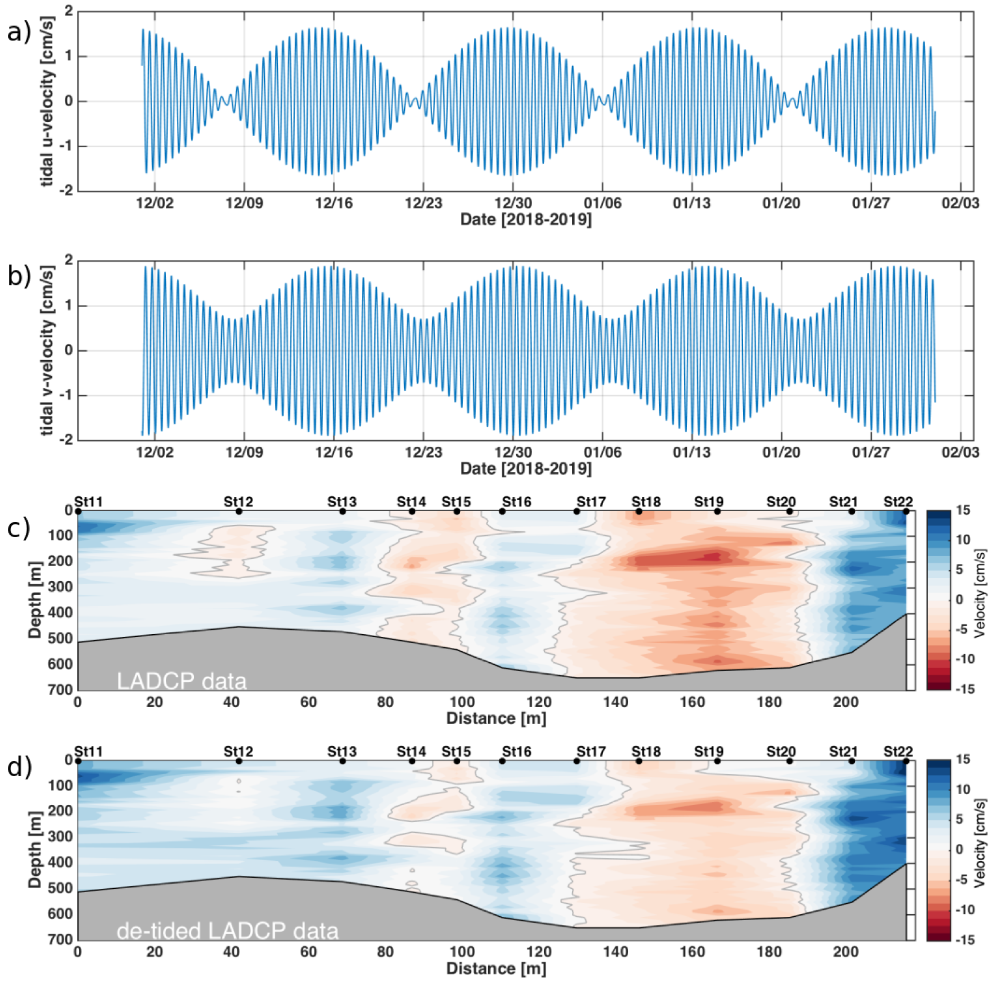

Figure A1. Tidal contributions to the LADCP data. (a) Zonal and (b) meridional velocity of tidal flow at station 11 from CATS2008 (Padman et al., 2002), see discussion in section 2.2. (c) LADCP velocities and (d) de-tided LADCP velocities across the Belgica Trough (stations 11 – 22).

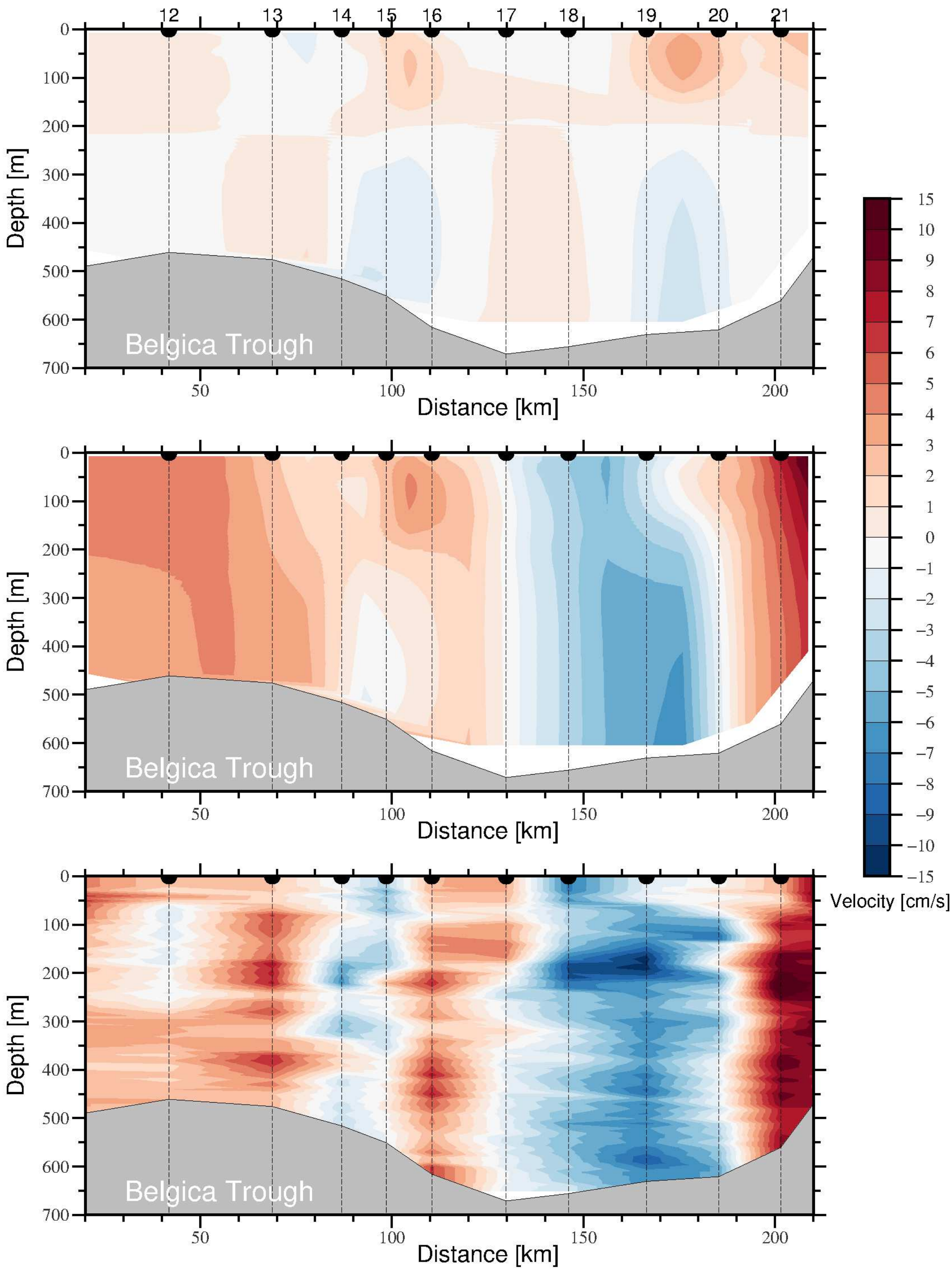

Figure A2. Flow across the Belgica Trough shelf-break section, stations 11 to 22. (a) Geostrophic velocity referenced to 300 m, roughly the top of the CDW layer. (b) Geostrophic velocity referenced to the LADCP data using a least squares fit across all depths?. c) Unreferenced velocity from LADCP data.

References

Armitage, T. W. K., Kwok, R., Thompson, A. F., & Cunningham, G. (2018). Dynamic topography and sea level anomalies of the Southern Ocean: Variability and teleconnections. *J. Geophys. Res.*, *123*, 613 – 630. (doi: 10.1002/2017JC013534)

Arneborg, L., Wåhlin, A. K., Björk, G., Liljebladh, B., & Orsi, A. (2012). Persistent inflow of warm water onto the central Amundsen shelf. *Nat. Geosci.*, *5*, 876–880. doi: 10.1038/ngeo1644

Assmann, K., Hellmer, H. H., & Jacobs, S. S. (2005). Amundsen Sea ice production and transport. *J. Geophys. Res*, *110*, C12013.

Biddle, L. C., Heywood, K. J., Kaiser, J., & Jenkins, A. (2017). Glacial Meltwater identification in the Amundsen Sea. *J. of Phys. Oceanorg.*, *47*, 933–954.

Biddle, L. C., Loose, B., & Heywood, K. J. (2019). Upper ocean distribution of glacial meltwater in the amundsen sea, antarctica. *J. Geophys. Res.*, *124*, 6854 – 6870. (doi:10.1029/2019JC015133)

Cook, A., & Vaughan, D. (2010). Overview of areal changes of the ice shelves on the Antarctic Peninsula over the past 50 years. *Cryosphere*, *4*, 77–98.

Couto, N., Martionson, D. G., Kohut, J., & Schofield, O. (2017). Distribution of Upper Circumpolar Deep Water on the warming continental shelf of the West Antarctic Peninsula. *J. Geophys. Res. Oceans*, *122*, 5306 – 5315. (doi:10.1002/2017JC012840)

Dinniman, M. S., & Klinck, J. M. (2004). A model study of circulation and cross-shelf exchange on the west Antarctic Peninsula continental shelf. *Deep Sea Res. Pt. II*, *51*(17-19), 2003–2022.

Dotto, T. S., Garabato, A. C. N., Bacon, S., Holland, P. R., Kimura, S., Firing, Y. L., ... Jenkins, A. (2019). Wind-driven processes controlling oceanic heat delivery to the Amundsen Sea, Antarctica. *J. Phys. Oceanogr.*, 2829 – 2849.

Dutrieux, P., Rydt, J. D., Jenkins, A., Holland, P., Ha, H. K., Lee, S. H., ... Schroeder, M. (2014). Strong sensitivity of Pine Island ice-shelf melting to climatic variability. *Science*, *343*, 174 – 178. (doi:10.1126/science.1244341)

Gade, H. G. (1979). Melting of ice in sea water: a primitive model with application to the Antarctic Ice Shelf and icebergs. *J. Phys. Oceanogr.*, *9*, 1890 – 198.

Gille, S. T. (2008). Decadal-scale temperature trends in the Southern Hemisphere ocean. *J. Climate*, *21*(18), 4749–4765.

Hellmer, H., Kauker, F., Timmermann, R., Determann, J., & Rae, J. (2012). Twenty-first-century warming of a large Antarctic ice-shelf cavity by a redirected coastal current. *Nature*, *485*, 225 – 228.

Holland, P. R., Jenkins, A., & Holland, D. M. (2010). Ice and ocean processes in the Bellingshausen Sea, Antarctica. *J. Geophys. Res.*, *115*, C05020.

IMBIE. (2018). Mass balance of the Antarctic Ice Sheet from 1992 to 2017. *Nature*, *558*, 219–222.

Jacobs, S. S. (1991). On the nature and significance of the Antarctic Slope Front. *Mar. Chem*, *35*, 9–24.

Jenkins, A., & Jacobs, S. (2008). Circulation and melting beneath George VI Ice Shelf, Antarctica. *J. of Geophys. Res.*, *113*, C04013. doi: doi:10.1029/2007JC004449

Jenkins, A., Shoosmith, D., Dutrieux, P., Jacobs, S., Kim, T. W., Lee, S. H., ... Stammerjohn, S. (2018). West antarctic ice sheet retreat in the Amundsen Sea driven by decadal oceanic variability. *Nature Geosci*, *11*, 733 - 738. (doi:10.1038/s41561-018-0207-4)

Joughin, I., Tulaczyk, S., Bindschadler, R., & Price, S. (2002). Changes in West Antarctic ice stream velocities: observation and analysis. *J. Geophys. Res.*, *107*, 2289.

Kalen, O., Assmann, K. M., Wahlin, A. K., Ha, H., Kim, T. W., & Lee, S. (2015). Is the oceanic heat flux on the central Amundsen Sea shelf caused by barotropic or baroclinic currents? *Deep-Sea Res. II*, *123*, 7 – 15. (doi: 10.1016/j.dsr2.2015.07.014)

Kim, I. (2016). The distribution of glacial meltwater in the Amundsen Sea, Antarctica. *J. Geophys. Res.*, *121*, 1654–1666.

Loose, B., Schlosser, P., Smethie, W. M., & Jacobs, S. (2009). An optimized estimate of glacial melt from the Ross Ice Shelf using nobel gases, stable isotopes and CFC transient tracers. *J. Geophys. Res.*, *114*, C08007.

Mathiot, P., Goosse, H., Fichefet, T., Barnier, B., & Gallee, H. (2011). Modelling the seasonal variability of the Antarctic Slope Current. *Ocean Science, European Geoscience Union*, *7*, 445 – 532. (doi: 10.5194/os-7-455-2011)

McTaggart, K. E., Johnson, G. C., Johnson, M. C., Delahoyde, F., & Swift, J. H. (2010). Notes on CTD/O data acquisition and processing using sea-bird hardware and software. *IOCCP Reports*, *Report No. 14*, ICPO Publication Series No. 134. (Version 1)

Moffat, C., Beardsley, R. C., Owens, B., & Van Lipzig, N. (2008). A first description of the Antarctic Peninsula Coastal Current. *Deep Sea Res. Part II*, *55*, 277–293.

Moffat, C., & Meredith, M. (2018). Shelf-ocean exchange and hydrography west of the Antarctic Peninsula: a review. *Phil. Trans. Roy. Soc. A*, *376*, 20170164. doi: 10.1098/rsta.2017.0164

Morlighem, M., et al. (2019). MEaSUREs BedMachine Antarctica, Version 1. *Boulder, Colorado USA. NASA National Snow and Ice Data Center Distributed Active Archive Center*. doi: https://doi.org/10.5067/C2GFER6PTOS4

Mosby, H. (1934). The waters of the Atlantic Antarctic Ocean. *The Norwegian Antarctic Expeditions*, *1*, 131.

Nakayama, Y., Menemenlis, D., Schodlok, M., & Rignot, E. (2017). Amundsen and Bellingshausen Seas simulation with optimized ocean, sea ice, and thermodynamic ice shelf model parameters. *J. Geophys. Res.*, *122*, 6180–6195.

Nakayama, Y., Menemenlis, D., Zhang, H., Schodlok, M., & Rignot, E. (2018). Origin of Circumpolar Deep Water intruding onto the Amundsen and Bellingshausen Sea continental shelves. *Nature Commun.*, *9:3403*, 1 – 9.

Nakayama, Y., Schröder, M., & Hellmer, H. H. (2013). From circumpolar deep water to the glacial meltwater plume on the eastern Amundsen shelf. *Deep Sea Res. Part I*, *77*, 50–62.

Nakayama, Y., Timmermann, R., Rodehacke, C. B., Schröder, M., & Hellmer, H. H. (2014). Modeling the spreading of glacial meltwater from the Amundsen and Bellingshausen seas. *Geophys. Res. Lett.*, *41*(22), 7942–7949.

Naveira-Garabato, A. C., Forryan, A., Dutrieux, P., Brannigan, L., Biddle, L. C., Heywood, K. J., … S., K. (2017). Vigorous lateral export of the meltwater outflow from beneath an Antarctic ice shelf. *Nature*, *542*, 219 – 222. (doi:10.1038/nature20825)

Orsi, A. H., Johnson, G. C., & Bullister, J. L. (1999). Circulation, mixing, and production of Antarctic Bottom Water. *Prog. in Oceanogr.*, 55 – 109.

Padman, L., Costa, D. P., Dinniman, M. S., Fricker, H. A., Goebel, M. E., Huckstadt, L. A., … others (2012). Oceanic controls on the mass balance of Wilkins Ice Shelf, Antarctica. *J. Geophys. Res.*, *117*. (C01010)

Padman, L., Fricker, H. A., R. Coleman, S. H., & Erofeeva, L. (2002). A new tide model for the Antarctic ice shelves and seas. *Annals of Glaciology*, *34*, 247 – 254.

Paolo, F. S., Fricker, H. A., & Padman, L. (2015). Volume loss from Antarctic ice shelves is accelerating. *Science*, *348*, 327–331.

Pena-Molino, B., McCartney, M. S., & Rintoul, S. (2016). Direct observations of the Antarctic Slope Current transport at 113°e. *J. Geophys. Res.*, *121*, 7390 – 7407. (doi:10.1002/2015JC011594)

Pritchard, H. D., Ligtenberg, S. R. M., Fricker, H. A., Vaughan, D. G., van den

Broeke, M. R., & Padman, L. (2012, 04 26). Antarctic ice-sheet loss driven by basal melting of ice shelves. *Nature*, *484*(7395), 502–505. Retrieved from http://dx.doi.org/10.1038/nature10968

Richardson, G., Wadley, M. R., Heywood, K. J., Stevens, D. P., & Banks, H. T. (2005). Short-term climate response to a freshwater pulse in the Southern Ocean. *Geophys. Res. Lett.*, *32*, L03702.

Rignot, E., Jacobs, S., Mouginot, J., & Scheuchl, B. (2013). Ice-shelf melting around Antarctica. *Science*, *341*, 266–270.

Rignot, E., Mouginot, J., Morlighem, M., Seroussi, H., & Scheichl, B. (2014). Widespread, rapid grounding line retreat of Pine Island, Thwaites, Smith, and Kohler glaciers, West Antarctica, from 1992 to 2011. *Geophys. Res. Lett*, *41*, 3502–3509.

Rignot, E., Mouginot, J., Scheuchl, B., van den Broeke, M., van Wessem, M. J., & Morlighem, M. (2019). Four decades of Antarctic Ice Sheet mass balance from 1979 – 2017. *PNAS*, 1095–1103.

Ruan, X., Speer, K., Thompson, A., & Schulze-Chretien, L. (2020). Ice-Shelf Meltwater Overturning Cell in the Bellingshausen Sea. *J. of Phys. Oceanogr.*, submitted.

Rye, C. D., Naveira-Garabato, A. C., Holland, P. R., Meredith, M. P., Nurser, A. J. G., Hughes, C. W., … Webb, D. J. (2014). Rapid sea-level rise along the Antarctic margins in response to increased glacial discharge. *Nat. Geosci.*, *7*, 732–735. (https://doi.org/10.1038/ngeo2230)

Savidge, D. K., & Amft, J. A. (2009). Circulation on the west Antarctic Peninsula derived from 6 years of shipboard adcp transects. *Deep Sea Res. Pt. I*, *56*, 1633–1655.

Schmidtko, S., Heywood, K., Thompson, A., & Aoki, S. (2014). Multidecadal warming of Antarctic waters. *Science*, *346*.

Stewart, A., & Thompson, A. (2015). Deep Water across the Antarctic shelf break. *Geophys. Res. Lett.*, *42*, 432–440.

St-Laurent, P., Klinck, J. M., & Dinniman, M. S. (2013). On the role of coastal troughs in the circulation of warm circumpolar deep water on Antarctic Shelves. *J. Phys. Oceanogr.*, *43*, 51 – 64. (doi: 10.1175/JPO-D-11-0237.1)

Swart, N. C., & Fyfe, J. C. (2013). The influence of recent Antarctic ice sheet retreat on simulated sea ice area trends. *Geophys. Res. Lett.*, *40*, 4328–4332.

Talbot, M. H. (1988). Oceanic environment of George VI ice shelf, Antarctic Peninsula. *Ann. Glaciol.*, *11*, 161–164.

Thompson, A., Schulze-Chretien, L., & Speer, K. (2020). Initiation of the Antarctic Slope Current in West Antarctica. *Geophys. Res. Let.*, submitted.

Thompson, A., Stewart, A. L., Spence, P., & Heywood, K. J. (2018). The Antarctic Slope Current in a changing climate. *Reviews of Geophysics*, *56*, 741 – 770. (doi:10/10292018RG000624)

Thurnherr, A. M., Jacobs, S. S., Dutrieux, P., & Giulivi, C. F. (2014). Export and circulation of ice cavity water in Pine Island Bay. *J. Geophys. Res. Oceans*, *119*, 1754 – 1764. (doi: 10.1002/2013JC009307)

Thurnherr, A. M., Visbeck, M., Firing, E., King, B. A., Hummon, J. M., Krahmann, G., & Huber, B. (2010). A manual for acquiring Lowered Doppler Current Profilier data. *In The GO-SHIP Repeat Hydrography Manual: A Collection of Expert Reports and Guidelines*, *Version 1, (eds E. M. Hood, C. L. Sabine and B. M. Sloyan*, 21. (IOCCP Report Number 14; ICPO Publication Series Number 134))

Wahlin, A. K., Kalen, O., Arneborg, L., Bjrk, G., Carvajal, G., Ha, H. K., … Stranne, C. (2013). Variability of warm deep water inflow in a submarine trough on the Amundsen Sea Shelf. *J. Phys. Oceanogr.*, *43*(10), 2054 – 2070. doi: 10.1175/JPO-D-12-0157.1

Walker, D. P., Brandon, M., Jenkins, A., Allen, J. T., Dowdeswell, J., &

Evans, J. (2007). Oceanic heat transport onto the Amundsen Sea shelf through a submarine glacial trough. *Geophys. Res. Let.*, *34*, L02602. (doi:10.1029/2006GL028154)

Walker, D. P., Jenkins, A., Assmann, K. M., Shoosmith, D. R., & Brandon, M. A. (2013). Oceanographic observations at the shelf break of the Amundsen Sea, Antarctica. *J. Geophys. Res.*, *118*, 2906–2918.

Webber, B. G. M., Heywood, K. J., Stevens, D. P., & Assmann, K. M. (2019). The impact of overturning and horizontal circulation in Pine Island Trough on ice shelf melt in the eastern Amundsen Sea. *J. Phys. Oceanogr.*, *49*(1), 63 – 83. doi: 10.1175/JPO-D-17-0213.1

Whitworth, T. I., Orsi, A. H., Kim, S.-J., Nowlin, W. D. J., & Locarnini, R. A. (1998). Water masses and mixing near the Antarctic Slope Front. *In Ocean, Ice, and Atmosphere: Interactions at the Antarctic Continental Margin*, *(eds S.S. Jacobs and R.F. Weiss)*. (doi:10.1029/AR07p0001)

Zhang, X., Thompson, A. F., Flexas, M., Roquet, F., & Bornemann, H. (2016). Circulation and meltwater distribution in the Bellingshausen Sea: from shelf break to coast. *Geophys. Res. Lett*, 6402 – 6409. doi: 10.1002/2016GL068998